Master's Thesis

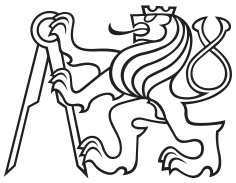

Czech Technical University in Prague

F3

Faculty of Electrical Engineering
Department of Measurement

Eddy Current Flaw Detector

Ondřej Fidra

Supervisor: prof. Ing. Radislav Šmíd, Ph.D.
May 2020

ZADÁNÍ DIPLOMOVÉ PRÁCE

I. OSOBNÍ A STUDIJNÍ ÚDAJE

Příjmení: **Fidra** Jméno: **Ondřej** Osobní číslo: **456869**

Fakulta/ústav: **Fakulta elektrotechnická**

Zadávající katedra/ústav: **Katedra měření**

Studijní program: **Kybernetika a robotika**

Studijní obor: **Senzory a přístrojová technika**

II. ÚDAJE K DIPLOMOVÉ PRÁCI

Název diplomové práce:

Detektor vad pomocí vířivých proudů

Název diplomové práce anglicky:

Eddy Current Flaw Detector

Pokyny pro vypracování:

Design and develop an eddy current flaw detector using the lock-in detection realized computationally in the microcontroller (e.g., STM32L4). Design the detector as a system consisting of a battery-powered handheld unit for detection and stationary unit for signal visualization and data processing. Use wireless communication such as Bluetooth to transfer data between the handheld and the visualization unit. Design and realize a differential eddy current probe and evaluate the performance of the system on samples with simulated cracks.

Seznam doporučené literatury:

[1] Shull, P. J.: Nondestructive Evaluation: Theory, Techniques, and Applications, CRC Press, 2002.
[2] STmicroelectronics datasheets
[3] Nondestructive Testing Handbook, Third Edition: Volume 5, Electromagnetic Testing (ET), ASNT 2004.

Jméno a pracoviště vedoucí(ho) diplomové práce:

prof. Ing. Radislav Šmíd, Ph.D., katedra měření FEL

Jméno a pracoviště druhé(ho) vedoucí(ho) nebo konzultanta(ky) diplomové práce:

Datum zadání diplomové práce: **23.01.2020** Termín odevzdání diplomové práce: _____

Platnost zadání diplomové práce: **30.09.2021**

prof. Ing. Radislav Šmíd, Ph.D. podpis vedoucí(ho) práce	podpis vedoucí(ho) ústavu/katedry	prof. Mgr. Petr Páta, Ph.D. podpis děkana(ky)

III. PŘEVZETÍ ZADÁNÍ

Diplomant bere na vědomí, že je povinen vypracovat diplomovou práci samostatně, bez cizí pomoci, s výjimkou poskytnutých konzultací. Seznam použité literatury, jiných pramenů a jmen konzultantů je třeba uvést v diplomové práci.

.	
Datum převzetí zadání	Podpis studenta

Acknowledgements

I would like to thank the supervisor prof. Ing. Radislav Šmíd, Ph.D. for his continuous support during this thesis. Furthermore, I would like to thank my parents for the constant positive mood and psychic support during the whole study.

Declaration

I hereby declare that I worked out the presented thesis independently, and I quoted all the sources used in this thesis in accord with Methodical instructions about ethical principles for writing an academic thesis.

In Prague, 22th May 2020

Prohlašuji, že jsem předloženou práci vypracoval samostatně, a že jsem uvedl veškeré použité informační zdroje v souladu s Metodickým pokynem o dodržování etických principů při přípravě vysokoškolských závěrečných prací.

V Praze, 22. května 2020

Abstract

In this thesis, the problematics of non-destructive testing of metal objects with eddy current is discussed. It also points on design, including the production of the wireless device with a standard microcontroller and with graphical data representation with the ability to set critical parameters. There is a socket to connect probes with various parameters. The development of several probes is discussed in details within the thesis. In the last, the possibility of wireless communication with a superior device is presented.

Keywords: Non-destructive testing, Eddy current, Flaw detection, Microcontroller

Supervisor: prof. Ing. Radislav Šmíd, Ph.D.

Abstrakt

V této práci je diskutována problematika nedestruktivního testování kovových předmětů pomocí vířivých proudů. Práce podrobněji popisuje celkový návrh i s výrobou bezdrátového zařízení s běžným mikrokontrolérem a s grafickým zobrazováním dat s možností nastavení důležitých parametrů. K připojení sondy se na zařízení nachází patice, která umožňuje jednoduchou výměnu sondy. V rámci práce bylo sestaveno několik kompatibilních sond, které jsou v práci probrány detailněji. V poslední části práce je probrána možnost bezdrátové komunikace měřícího zařízení s nadřazeným systémem.

Klíčová slova: Nedestruktivní testování, Vířivé proudy, Detekce vad, Mikrokontrolér

Překlad názvu: Detektor vad pomocí vířivých proudů

Contents

Figures

Chapter 1

Introduction

The field of non-destructive testing (NDT) is a very broad, interdisciplinary field that plays a critical role in assuring that structural components and systems perform their function reliably and cost-effectively. NDT technicians and engineers define and implement tests that locate and characterise material conditions and flaws. These flaws can lead to a critical collapse of the construction, and in many cases, the property can be damaged or, the people's lives can be in danger. The tests are performed in a manner that does not affect the future usefulness of the object or material. In other words, NDT allows parts and material to be inspected and measured without damaging them. Because it allows inspection without interfering with a product's final use, NDT provides an excellent balance between quality control and cost-effectiveness [5].

The NDT is divided into separate species according to the physical phenomenon and methods it uses. Many people are already familiar with some of the technologies that are used in NDT from their uses in the medical industry. Most people have also had an X-ray taken, and many mothers have had ultrasound used by doctors to give their baby a checkup while still in the womb. X-rays and ultrasound are only a few of the technologies used in the field of NDT [5].

The significant improvement in NDT was made in terms of digital signal processing (DSP), in comparison from the past. This growth in DSP means more flexibility and options in words of mathematical principles which are implemented in a code of microprocessor. It allows designing electronic structures of the devices using a small number of discrete elements.

As we take a look at the measuring systems for NDT, especially eddy current testing, their constructions are basically the same. Most of the systems consist of a desktop unit with a connected probe. The unit has all of the electronics required to measure, compute and represent data. There are a display and interacting elements which offer a set of the parameters of the measurement via the generated user interface. It also provides data representation in the form of a graph. The second part of the measurement system is the probe, which is connected to the central unit using connectors and some sort of cable. With the probe, the equipment operator is moving on the surface of the measured construction. By its signal, the device represents the computed data on display. The signal corresponds to a condition of the measured material.

Chapter 2

Aims

This thesis aims to design and develop an eddy current flaw detector using the lock-in detection realised computationally in the microcontroller. The detector will be consisting of a handheld, wireless and battery-powered device and desktop stationary visualisation unit. The wireless communication will be used to transfer data between the stationary and portable unit. Within the thesis, the design of eddy current detecting probes and evaluation of their performance will be tested on artificial flaws.

This thesis describes the process of a development measurement system for non-destructive testing using eddy current. The system can be divided into three essential parts, and their interconnection makes the working solution. One part is focused on designing and making measurement probes for the system. These probes are differential type consisting of three coupled coils. Another part is the electronic hardware which deals with electronics components for the system, designing the electric schematic and printed circuit board (PCB) of the device. In this part is included plastic mechanical construction designed in a 3D system and printed on the 3D printer. The last part describes the software in programmable components of the system. The microcontroller has to be able to provide requested functions from the computation view, but also from the hardware equipment.

2.1 Device

The fully operating system has to show an impedance plane diagram where the path of imaginary and real component of the received signal is displaying. So the device will have a graphical display. Another requirement on the device is that it must be wireless, and it has to be handheld. The device must have a possibility to send data to remotely to a superior device. To solve these requirements, the battery, battery management and some wireless module must be there. For the measurement itself, there must be components, which will drive the transmitting coil and which will convert and normalise the signal from the receiving coil. There will be a connector to attach the probes. Every component has to be controlled, and for this task, there will be a microcontroller (MCU). It has to generate a signal for the transmitting coil. Meanwhile, it has to capture a signal from receiver coils. After that capturing, the MCU will compute real and imaginary component from it, and draw the path on display how the components are changing, or send the result via wireless communication. These assignments are controlled by software in the MCU. There will be implemented lock-in amplifier in the MCU to compute the result.

2.2 Probes

As was mentioned earlier, the device works with a differential coil. The analysis of various designs and their evaluation is made within the thesis. The aim is on making coil itself, which can be separated in steps. The differential coil consists of two receiving coils and one transmitting coil. These receiving coils are wound on the ferrite cores and placed next to each other with a thin air gap between them. On this construction is wound transmitting coil. Between the receiving coils and the transmitting coil can be placed grounded shielding. The parameters of the coils are critical for sensitivity and working frequency.

Chapter 3

Non-destructive testing

The basic idea of non-destructive testing (NDT) is following. To determine the quality or integrity of an item nondestructively, simply find a physical phenomenon (the interrogating parameter) that will interact with and be influenced by your test specimen (the interrogated parameter) without altering the specimen's function.[18] Various technologies and methods are used to fulfil this requirement. The term Non-destructive testing (NDT) is linked with some technical terms. Let's introduce them first:[18]

- Non-destructive Testing (NDT) generally refers to the actual test only.
- Nondestructive Evaluation (NDE) implies not only the test but also its role in the process. This is the most general definition among all the terms.
- Nondestructive Examination (NDE) is typically used in areas other than process control.
- Nondestructive Inspection (NDI) is, like non-destructive examination, typically used in areas other than process control.
- Nondestructive Characterization (NDC) refers to the specific characterisation of material properties. NDC, of all the references, probably has the most restricted use.
- Non-destructive Sensing (NDS) generically refers to the use of sensors to derive information nondestructively. Here there is no specific implication

Some of these terms are interchangeable in practice. In this thesis, the term NDT is used to imply the problematics. The NDT uses various measuring methods to enlarge a set of measurable materials and their defects. These methods can be sorted into six categories. They are:[8]

- Visual and Optical Testing (VT)
- Penetrant Testing (PT)
- Magnetic Particle Testing (MT)
- Electromagnetic Testing (ET) or Eddy Current Testing (ECT)
- Radiography (RT)
- Ultrasonic Testing (UT)

VT is based on looking for a defect by a human's eyes. The tools used in this type of testing are microscopes, magnifying glasses, mirrors etc. At basically the PT is the same base as the VT. In compare, it uses special fluorescent dye. The material is coated with a dye, once it dries the dye is removed, and remaining dye is trapped in imperfections of the material. The objects are then controlled by ultraviolet (UV) light and operator's sight. MT is based on imperfection distortion of the magnetic field of ferromagnetic material around the defects. Ferromagnetic dust is used as a testing medium. The medium is cumulated around the defects of the material, and it makes visual identification of the defect. ECT uses eddy currents, which are induced in testing material. These eddy currents are excited by alternating current in a coil. The non-homogeneities affect the direction and amplitude of eddy currents. The eddy currents are sensed by receiving coils and processed by instrumentation. RT techniques are used to show the penetration of the X-rays through the subject. The result is a shadowgraph of a part. It is commonly known in hospitals to show broken bones, for example. UT works with the propagation of the ultrasonic wave in the material. The defects in the material make echos, which are sensed by a receiver. A particular sort of UT is acoustic emission testing. It measures the acoustic emissivity of the stressing structure.[8]

This thesis works only with ECT, which is discussed in more detail.

3.1 Eddy current testing

The basic idea of ECT is in the measurement of the eddy current induced in the material by an alternating magnetic field. With this principle, the inspection of multiple parameters can be done, for example, cracks and non-homogeneities of the material can be found, the thickness of the top layer of paint can be estimated, the conductivity of the material can be measured. There are more techniques of how to measure with ECT described below.

3.1.1 Basic principle

The alternating magnetic field is generated by a coil, which is exited by alternating current. In the inspected metal are induced eddy currents. These currents interact with the opposite force to the excitation energy. Thus, the parameters of magnetic circuit changes and parameters of excitation coil changes. This phenomenon is named mutual inductance. When a defect appears on the affected area of eddy currents, the parameters change in comparison of non-defected area. These differences are captured. The interaction between the measuring coil and measuring material is represented in Fig. 3.1 (adapted from [7]).

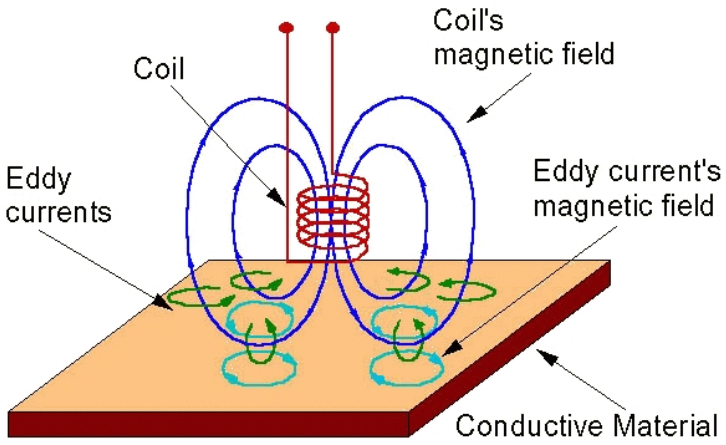

Figure 3.1: Mutual inductance of coil and material

This principle is used in more forms of ECT. Specific measurements differ by excitation waveforms, frequency, type of probe and with signal processing.

With the ECT is linked term depth of penetration. It defines how the

current density in the inspected material is spread. Eddy current density decreases exponentially with depth. This phenomenon is known as the skin effect. The depth that eddy currents penetrate into a material is affected by the frequency of the excitation current and the electrical conductivity and magnetic permeability of the specimen.[6] The ECT defines multiple depths of penetration. Where the current density decreases to 37% ($\frac{1}{\exp}$), the standard depth is defined. The second standard depth of penetration is defined in 13.5% of the current density, and the third is defined in 5% of the current density. The standard depth of penetration can be computed from the following formula:[6]

$$\delta = \frac{1}{\sqrt{\pi f \mu \sigma}} \tag{3.1}$$

where δ is standard depth of penetration $[mm]$, f is frequency $[Hz]$, μ is magnetic a permeability $[\frac{H}{mm}]$ and σ is electrical conductivity $[\%IACS]$.[6] The representation of the depth of penetration is in Fig. 3.2 (adapted from [6]).

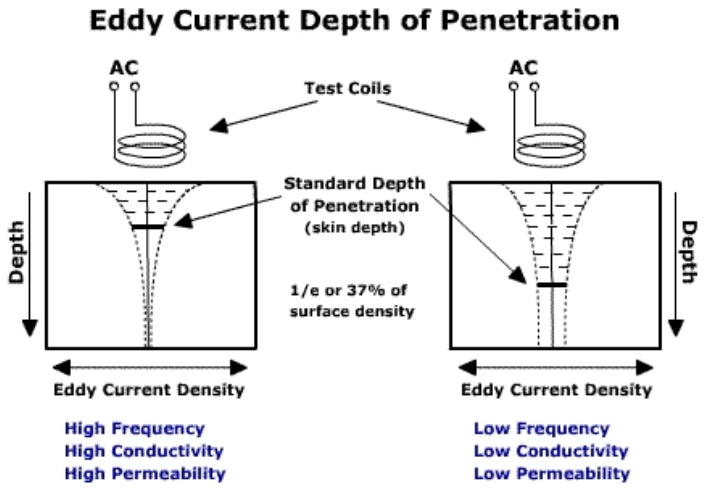

Figure 3.2: Representation of depth of penetration

The received signal changes compared to the reference excitation signal. If the excitation signal is harmonical, a phase-shift and an amplitude-shift are taken to an account. Lock-in amplifier process these types of signals. If the excitation signal was not harmonical (usually square signal or pulses) the difference is in the shape of the received signal. It can be processed with likelihood algorithms or artificial intelligence.

3.1.2 ECT Probes

Sensing the above mentioned phenomenal can be done with various probes. Between basic types of probes belongs absolute probes and differential probes. The details of these probes are described below. These types can have many possible constructions. Their coils can be wounded on ferromagnetic cores, and they can be shielded, they can differ in sizes etc.

Absolute

This type of probe consists of one wounded coil. The coil serves as an excitation coil. The signal from a generator is connected to the probe, so the probe has voltage and through it flow current. These two quantities are sensed and processed. As the probe is passing different environments, its parameters are changing. This causes the change of voltage and flowing current. An absolute probe is shown in Fig. 3.3 (adapted from [10]).

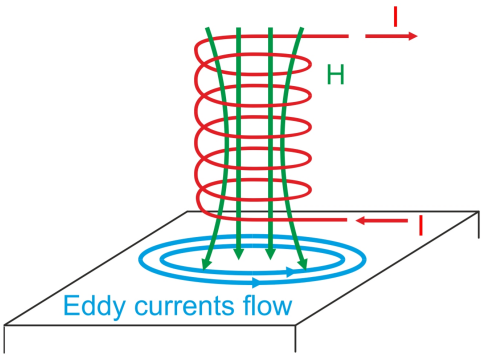

Figure 3.3: Construction of the absolute probe

Differential

Differential probes are more sophisticated than the absolute probes. They consist of two receiving coils and one transmitting (excitation) coil. The receiving coils have ideally the same parameters, and they are placed next to each other. The excitation coil is wounded around the receiving coils. While the coil passes through the material with flaws, the induced voltages of receiving coils differ. The receiving coils are connected anti-serial, so the induced voltages are subtracted. Because of that, the sensitivity of these coils

is better than the sensitivity of absolute coils. This thesis is aimed to design and manufacture this type of coil. There exist probes, only with two coils, which acts as excitation coils. The signal evaluation is done the same way as a signal from absolute probes. Construction of the differential probe is shown in Fig. 3.4 (adapted from [10]).

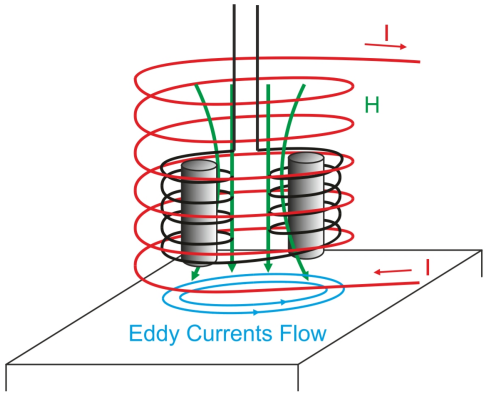

Figure 3.4: Construction of the differential probe

3.1.3 Lock-in amplifier

When the excitation signal is harmonical, the evaluation of the signal is done by the lock-in amplifier (LIA). In general, LIA's task is to filter the desired signal from the surrounding noise. In many cases, the amplitude of the noise is more significant than the amplitude of the required signal.[1] Block diagram of the lock-in amplifier is in Fig. 3.5 (adapted from [12]).

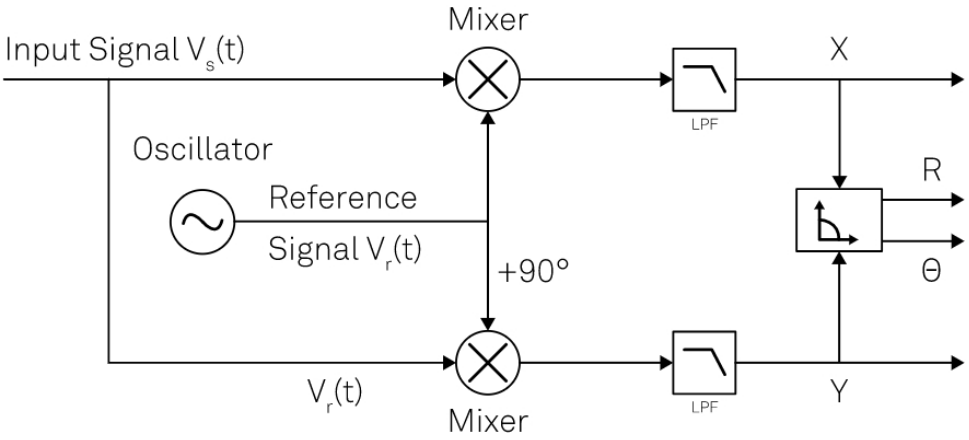

Figure 3.5: Block diagram of lock-in amplifier

As can be seen, the reference signal is used for excitation, and it is used for the processing of the received signal. In the processing part, the reference is divided into two signals. One is in phase with the reference, and the other is phase-shifted of ninety degrees. The received signal is multiplied by these two references. This step creates two signals with the various mean value obtained by two low-pass filtres which follows by the multipliers. The filtering creates an in-phase (I) and quadrature (Q) components (or real and imaginary) of the signal in relation to the reference. In ECT, the I and Q signal are displayed into the impedance plane diagram. The mathematics which defines this process is described below (adapted from [4]). The input signal can be desribed as equation (3.2).

$$U_{in} = U_{signal} \cos(\omega_{ref} t + \Theta_{signal}) \tag{3.2}$$

where U_{in} is received signal, U_{signal} is amplitude of the signal, ω_{ref} is radian frequency of received signal, t is time and Θ_{signal} is phase of received signal.

Two reference signals are defined by equasion (3.3) and (3.4).

$$U_{refsin} = U_{ref} \sin(\omega_{ref} t) \tag{3.3}$$
$$U_{refcos} = U_{ref} \cos(\omega_{ref} t) \tag{3.4}$$

Now, the U_{signal} (3.2) is multiplied with U_{refsin} (3.3) and U_{refcos} (3.4). Obtained equations (3.5) and (3.6).

$$U_I = U_{in} U_{refcos} =$$
$$= \frac{1}{2} U_{signal} U_{ref} \cos(\Theta_{signal}) + \frac{1}{2} U_{signal} U_{ref} \cos(2\omega_{ref} t + \Theta_{signal}) \tag{3.5}$$
$$U_Q = U_{in} U_{refsin} =$$
$$= \frac{1}{2} U_{signal} U_{ref} \sin(2\omega_{ref} t + \Theta_{signal}) - \frac{1}{2} U_{signal} U_{ref} \sin(\Theta_{signal}) \tag{3.6}$$

When these signals are passes thought the low-pass filter, the in-phase and quadrature signal is obtained. Equations (3.7) and (3.8) represents this step.

$$I = \frac{1}{2} U_{signal} U_{ref} \cos(\Theta_{signal}) \tag{3.7}$$
$$Q = \frac{1}{2} U_{signal} U_{ref} \sin(\Theta_{signal}) \tag{3.8}$$

The I is in-phase component and the Q is quadrature component of the received signal.

Lock-in amplifier can be realised from discrete components, or it can be implemented in software. Let's focus on realising it by software. Assume that we have the hardware, which is generating a reference signal to the device under test (DUT) and sampling the received signal. The sampling rate

of the input signal must be the same as the sampling rate of the reference. For the multiplying, we need reference signal in-phase and ninety degrees phase-shifted signal. It can be done by shifting array which stores the data for the reference signal. The corresponding samples are multiplied. Then, the mean values through whole arrays are computed, to get the I and Q components from the multiplied arrays. A block diagram of digital lock-in is in Fig. 3.6 (adapted from [11]).

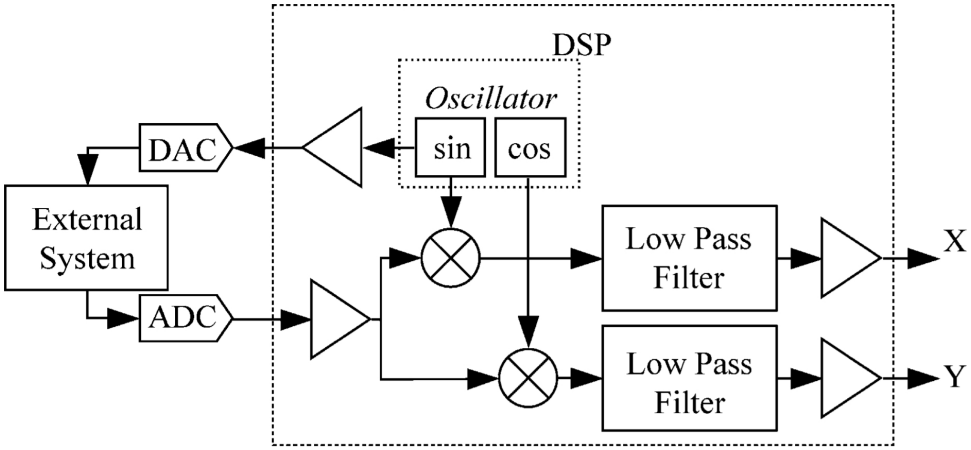

Figure 3.6: Block diagram of digital lock-in amplifier

Chapter 4

Hardware

The physical part of the measuring device can be divided into a mechanic and electronic part. This chapter describes the elements of these two parts in a detailed plane. The mechanical part of the device is built onto a double-sided printed circuit board (PCB). There is placed rotary encoder, which acts as an interacting element of the device. On the opposite side is soldered a pin header, which is used as a connector for the probes. There is also mounted a 3D printed plastic construction with the battery holder. The electronics part is made of surface mounted devices (SMD) which are soldered on the PCB, that electrically connect the components.

4.1 Microcontroller

The central component of the measuring device is a microcontroller (MCU). In general, an MCU consists of a processor core, random-access memory (RAM), read-only memory (ROM), data buses and many peripheral circuits in one package. It stands for every data processing, or data transfer, and it can interact with the surrounding parts thanks to its peripherals. In this work, the MCU is used to generate a signal to the transmitting coil, convert and process the waveform from the receiving coils and represent the results on display, eventually, send it via Bluetooth. The device is primarily battery-powered, and because of that reality, the low-power MCU was chosen. The MCU with the right peripherals and parameters was needed to accomplish these specific requirements. The picked MCU is made by STMicroelectronics, from their low-power family, it is ST32L475RGT6.

4.1.1 Overall description

The microcontroller mentioned above is based on ARM® Cortex®-M4 32-bit central processing unit (CPU) core with a floating-point unit (FPU), adaptive real-time accelerator (ART Accelerator^{TM}) and digital signal processing (DSP) instructions[22]. Flash memory of the MCU is 1MB large, and the operational memory (RAM) has 128kB. It has ultra-low-power features, which enable to reduce the MCU power consumption to 30nA.[22] The MCU is in an LQFP-64 package. An overview look at what the MCU includes is shown in a simplified block diagram at Fig. 4.1 (adapted from [21]).

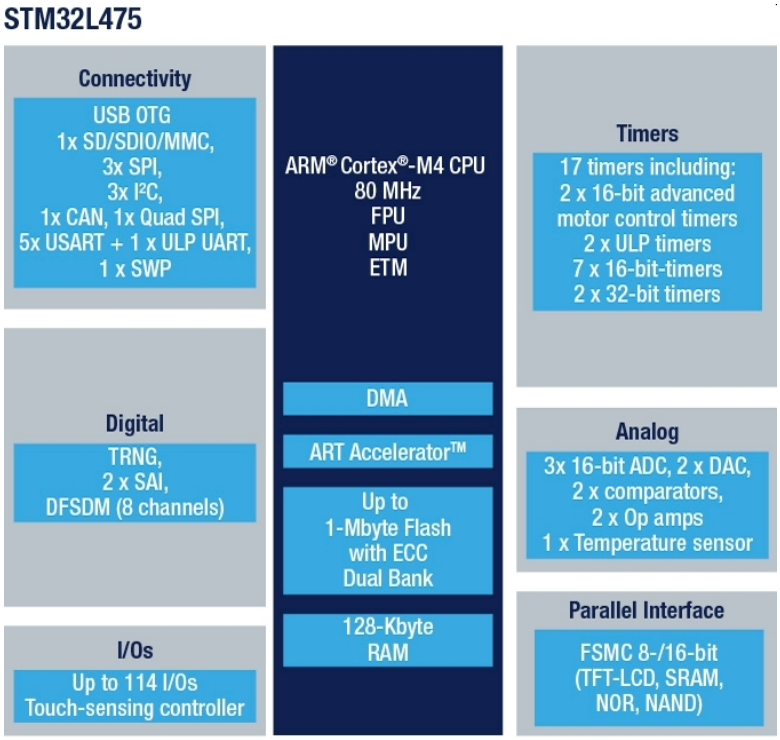

Figure 4.1: STM32L475RG components diagram

4.1.2 Peripherals

The MCU has a lot of peripherals and features. There are mentioned only the crucial parts for the application such as digital to analog converter (DAC) for signal generating, analog to digital converter (ADC) for signal sampling, direct memory access (DMA) for autonomous data transfer between peripherals and memory, timers for various usages, serial peripheral interface (SPI) to communicate with the display, universal synchronous/asynchronous receiver-transmitter (USART) to react with Bluetooth module and extended interrupts

and events controller (EXTI) to capture interaction from the rotary encoder.

DAC

There are two 12-bits voltage output DAC. Block schematic of DAC peripheral is shown in Fig. 4.2 (adapted from [23]). In the thesis is used only one DAC as a generator of waveforms for the excitation coil. The DAC is configured with DMA transfer data RAM, where are loaded waveform points, with conversion on the external trigger from the timer, which generates the sample rate. The basic DAC features are listed below:[22][23]

- 8-bit or 12-bit output mode
- Buffer offset calibration (factory and user trimming)
- Noise-wave generation
- Triangular-wave generation
- DMA capability for each channel
- External triggers for conversion

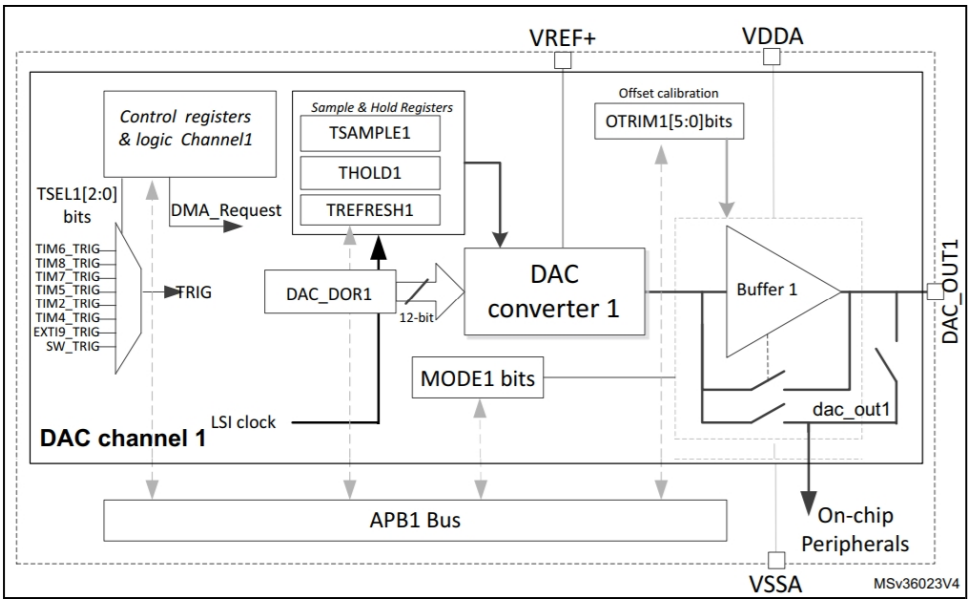

Figure 4.2: Block diagram of DAC peripheral

ADC

The device has three embedded successive approximation ADCs. Every ADC has 12-bit resolution. Simplified block diagram of the converter is in Fig. 4.3 (adapted from [23]). The thesis uses two ADCs. One is used for sampling the signal from the receiver coil. It is configured to simultaneously sample data with DAC. That means that is used the same timer to trigger ADC. After the sampling is done, the data are transferred via DMA to RAM. The essential features of ADCs are the following:[22][23]

- 12, 10, 8 or 6-bit configurable resolution
- Self-calibration
- 5.33 Msps maximum conversion rate with full resolution
- Up to 16 external channels
- Oversampling ratio adjustable from 2 to 256
- Start-of-conversion can be initiated by hardware or software
- 3 analog watchdogs per ADC

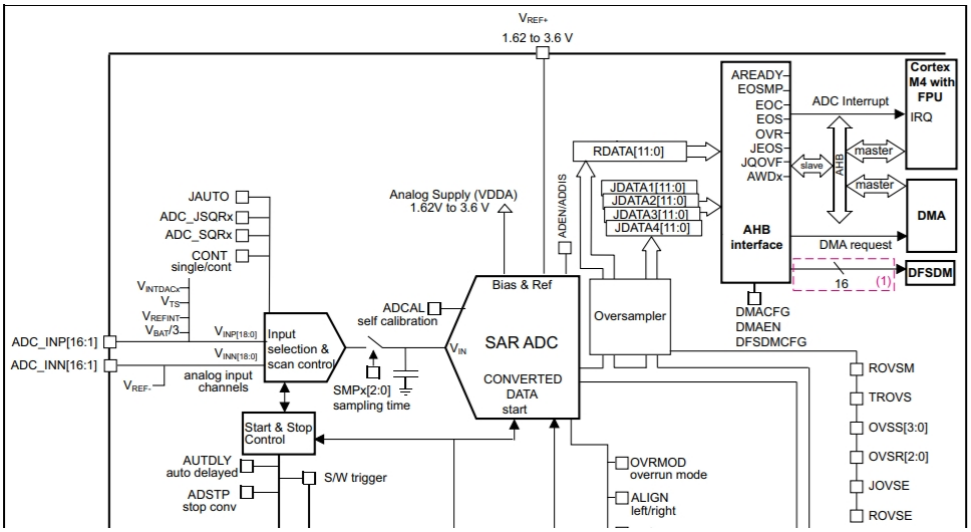

Figure 4.3: Simplified block diagram of ADC peripheral

DMA

As was mentioned above, ADC and DAC peripherals use DMA. DMA is connected on bus matrix and peripherals and can control the flow of the data

between peripheral and memory or between memory and memory independently on the activity of the CPU, so the CPU is free for other operations.[22] The MCU has two DMAs. Block diagram of the interconnection of the DMA in the MCU is in Fig. 4.4 (adapted from [23]). Main features of the DMA controller are listed below:[22][23]

- 14 independently configurable channels (requests)
- Each channel is connected to dedicated hardware DMA requests
- Support of transfers from/to peripherals to/from memory with circular buffer management
- Programmable priorities between requests from channels of one DMA (4 levels)
- Transfer size of source and destination are independent (byte, half-word, word)
- Generation of an interrupt request per channel

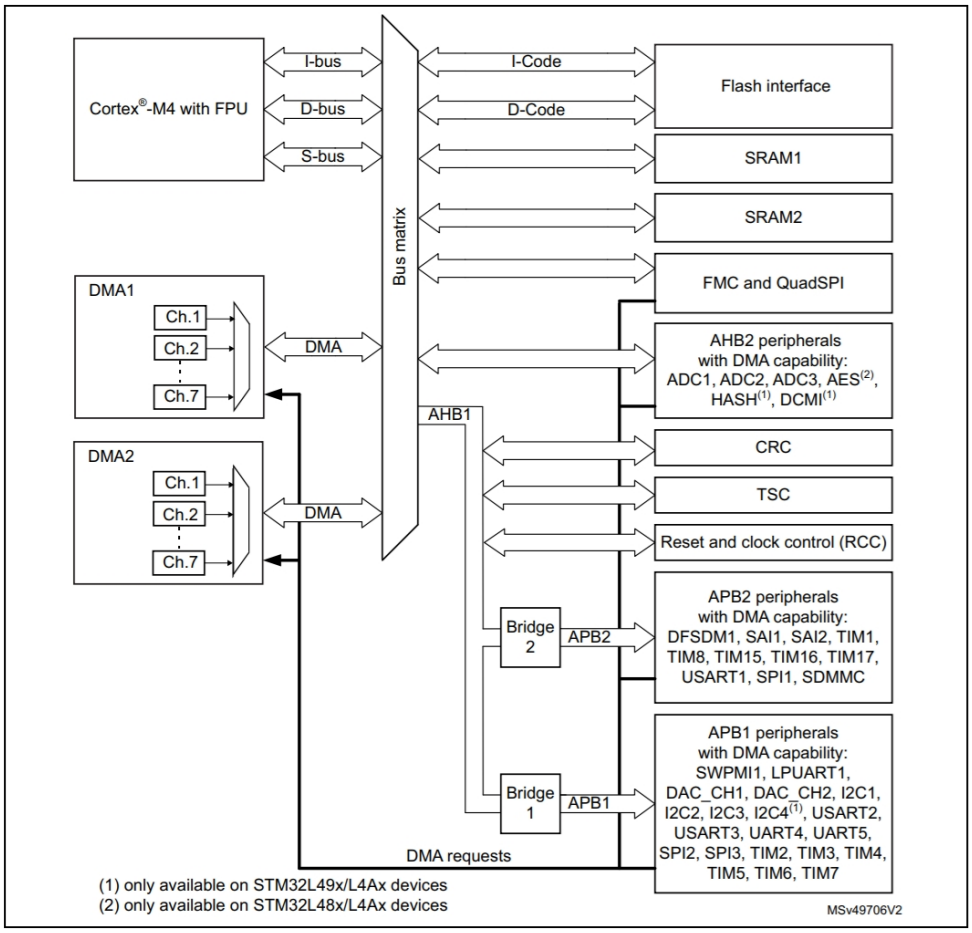

Figure 4.4: Block diagram of DMA peripheral

Timers

Three timers are enabled in the device. Two of these timers are used for ADC-DAC chain. One is generating pulses for DAC to trigger the DMA memory read, and the second is triggering sampling of ADC. The last timer is used for managing events of the rotary encoder. In this article, only the basic timers are discussed. The particular cases of timers usage are described in the software section. The MCU has 16 timers with various features. The block diagram of basic timers is visible in the Fig. 4.5 (adapted from [23]). When the timer is enabled and clocked over programmable prescaler, it counts the pulse in CNT counter up to a value saved in the auto-reload register (ARR). Once the value of the CNT reaches the value of ARR, the event is generated. The features of basic timer are:[22][23]

- 16-bit auto-reload upcounter

- 16-bit programmable prescaler used to divide by any factor between 1 and 65535
- Synchronization circuit to trigger the DAC
- Interrupt/DMA generation on the update event: counter overflow

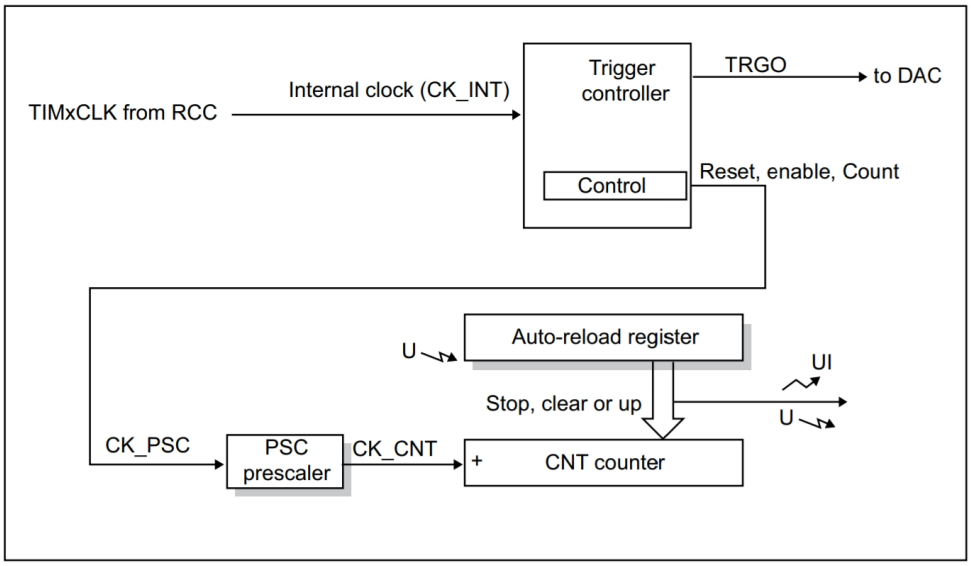

Figure 4.5: Block diagram of basic timer

SPI

Serial peripheral interface embedded in the MCU supports communication via SPI protocol. Block diagram of SPI of the MCU is shown in the Fig. 4.6 (adapted from [23]). The only component, which communicates via SPI with MCU is the display. In this case, a uni-directional mode is used. The LCD is a slave and MCU is configured as master and controls the data flow and generates a clock ticks. In the MCU there are three SPI peripherals. Its main features are following:[22][23]

- Master or slave operation
- Full-duplex, half-duplex or simplex synchronous transfers
- 4 to 16-bit data size selection
- Communication up to 40 Mbits/s in master and up to 24 Mbits/s slave
- Multimaster mode capability

- Programmable clock polarity and phase
- Programmable data order with MSB-first or LSB-first shifting
- Hardware CRC feature

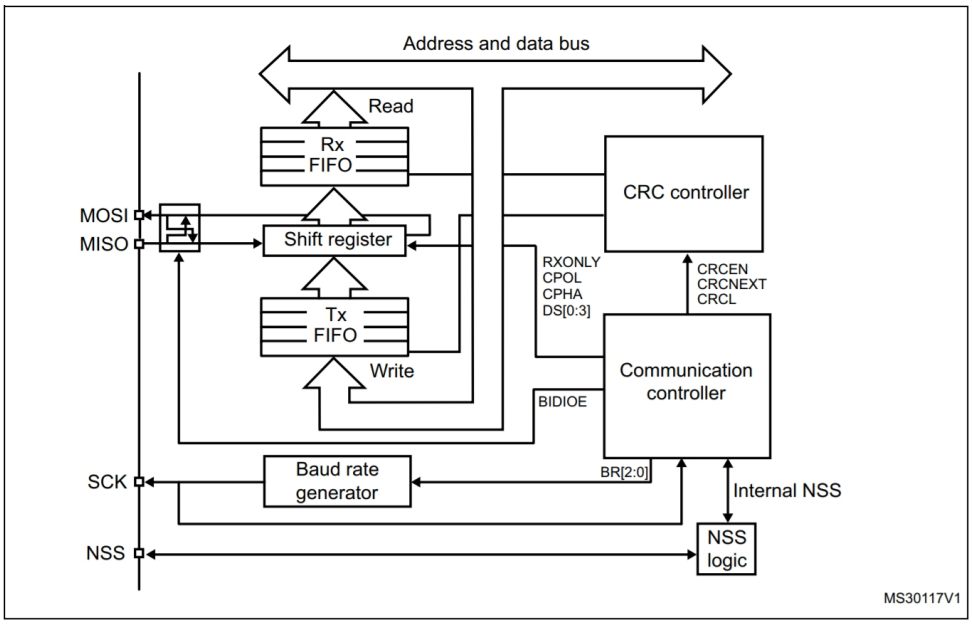

Figure 4.6: Block diagram of SPI peripheral

USART

Used Bluetooth module is communicating with the system via asynchronous serial communication named universal synchronous/asynchronous receiver-transmitter (UART). In this case, only receiver (RX) and transmitter (TX) signals are used. The Bluetooth module emulates console, and its configuring is done using commands coded in American standard code for information interchange (ASCII). The peripheral block diagram of the built-in peripheral is shown in the Fig. 4.7 (adapted from [23]). USART's basic features are:[22][23]

- Full-duplex asynchronous communications
- Configurable oversampling method
- A common programmable transmit and receive baud rate of up to 10 Mbit/s
- Auto baud rate detection

- Programmable data word length (7, 8 or 9 bits)
- Synchronous mode and clock output for synchronous communications
- Swappable Tx/Rx pin configuration
- Parity control
- Fourteen interrupt sources with flags

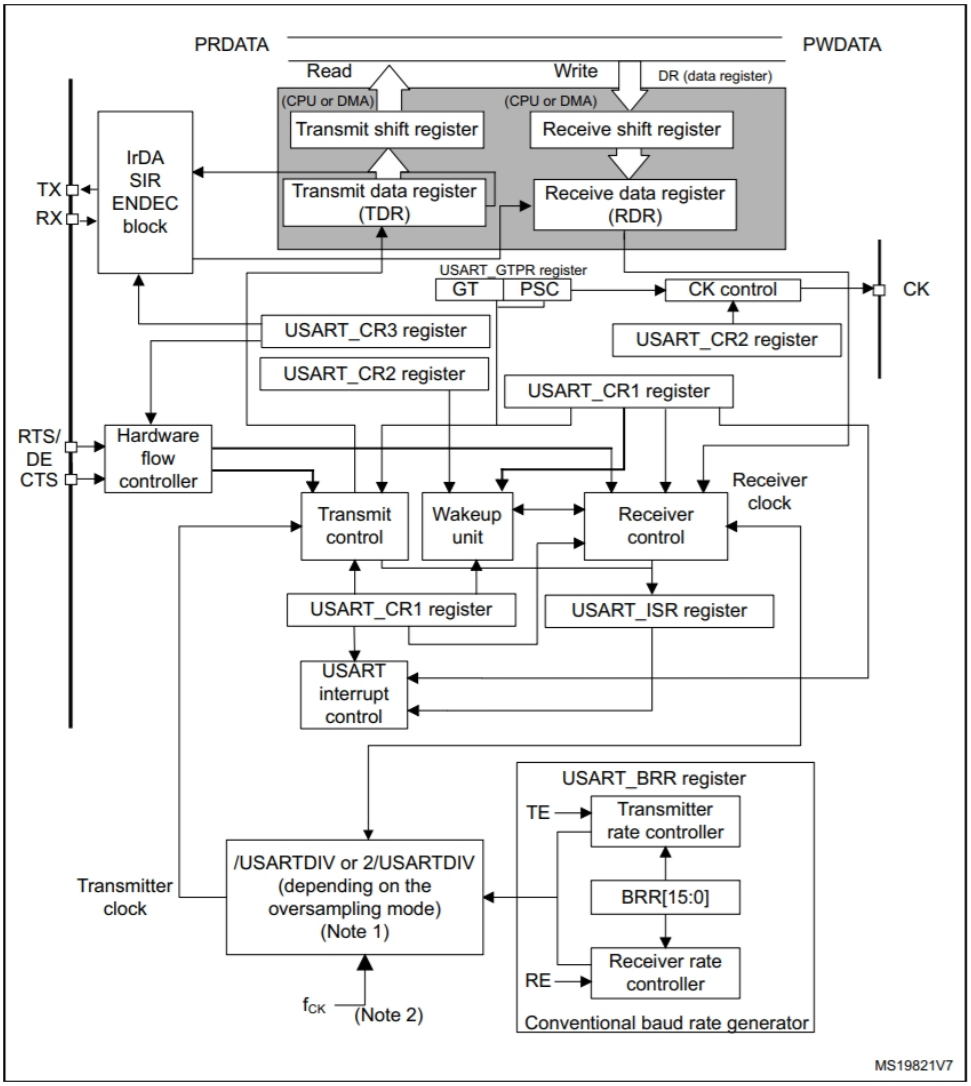

Figure 4.7: Block diagram of USART peripheral

EXTI

There is a rotary encoder to control the device which is connected directly on the MCU. These pins have configured pull-up resistors. The controlling

events, as rotate left, rotate right and push, are asynchronous. The MCU has peripheral named Extended interrupts and events controller (EXTI), which can catch these asynchronous signals and make an interrupt in the MCU. In comparison with the cyclical testing of pins states, this solution with interrupts saves CPU time. The diagram of EXTI is shown in Fig. 4.8 (adapted from [23]). Its main features are following:[22][23]

- Generation of up to 40 event/interrupt requests
- 26 configurable lines
- Independent mask on each event/interrupt line
- Configurable rising or falling edge (configurable lines only)
- Dedicated status bit (configurable lines only)
- Emulation of event/interrupt requests (configurable lines only)

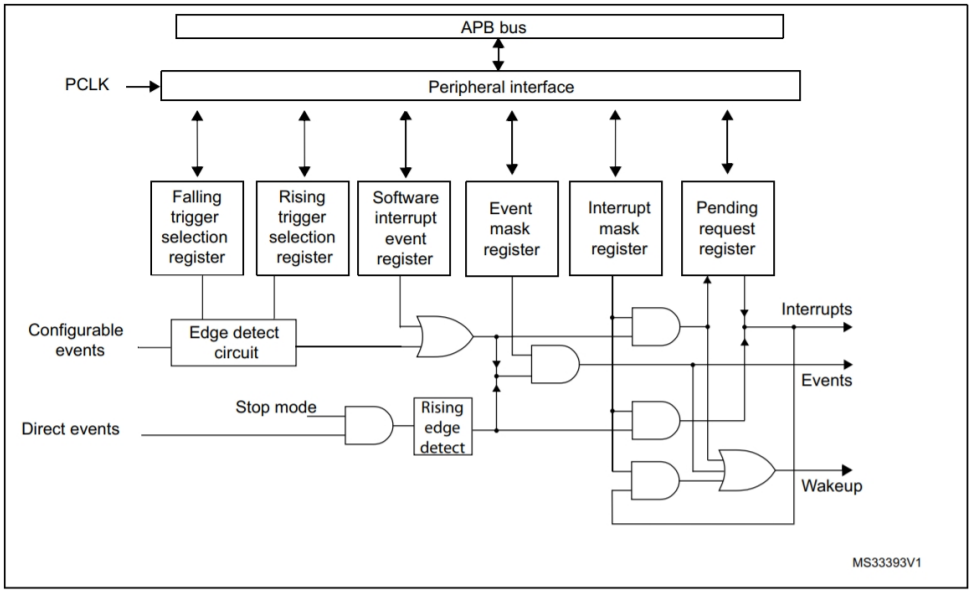

Figure 4.8: Block diagram of EXTI peripheral

4.2 Signal amplifiers

There are needs on parameters of output and input signals. The operational amplifiers (op-amp) are used to norm the signals. For the excitation of the transmitting (TX) part of a probe, the impedance matching is needed, because the output buffer of the DAC converter is weak. On the receiving

(RX) side, the signal has a variable amplitude and mismatching the design of input norming amplifier could mean lousy resolution of the measurement. The electronic schematic of signal amplifiers for TX and RX signals are shown in Fig. 4.9

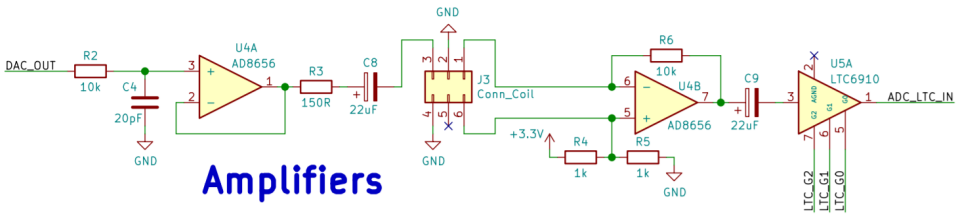

Figure 4.9: Schematic of TX and RX amplifiers

4.2.1 Transmitting

Because of the weak DAC output buffer on the MCU, the external buffer is needed. It is done using an operational amplifier with these requirements: low-voltage powered, rail-to-rail output, the possibility for the single polarity powering and enough current output. The chosen op-amp is AD8656 by Analog Devices. Basic features of this component are the following:[2]

- 2.7 V to 5.5 V operation
- Rail-to-rail input/output
- Bandwidth: 28 MHz

The op-amp is connected as a voltage follower. Input has an RC low-pass filter, to filter the higher harmonics from the DAC convertor. The cutoff frequency was examined from the highest sampling frequency of DAC to $500kHz$. The output buffer of the DAC has $5k\Omega$ resistance. The computation is in equation (4.1).

$$f_c = \frac{1}{2\pi RC} = \frac{1}{2\pi \cdot (10000 + 5000) \cdot 20 \cdot 10^{-12}} = 531kHz \qquad (4.1)$$

On the output of it is connected resistor to limit the output current and electrolytic capacitor to filter the DC component of the signal.

4.2.2 Receiving

The significant variance of the amplitude of the RX signal is the biggest deal of the RX amplifier part. It consists of two stages. The first stage is made by current-to-voltage converter realised by the standard op-amp. Choose op-amp is AD8656. The second stage is used to amplify the output signal of the converter. Because of variable amplitude, the op-amp with a digitally selectable gain was needed. The chosen is LTC6910-10 made by Analog Devices. Its basic features are listed below:[3]

- Single or Dual Supply: 2.7V to 10.5V Total
- Rail-to-rail input/output
- Bandwidth: 11 MHz
- 3-Bit Digital Gain Control in Three Gain-Code Options
- Selectable gains of 0, 1, 2, 5, 10, 20, 50 and 100V/V

4.3 Power management

The thesis aims at the design of a portable, battery-powered measuring device. Its power circuit must contain elements to charge the battery correctly and regulate the voltage from the battery in every condition. There is also a requirement for the reduction of power consumption. This section describes elements of the device's power management and its interconnection. The whole schematic of power management of the device is in Fig. 4.10

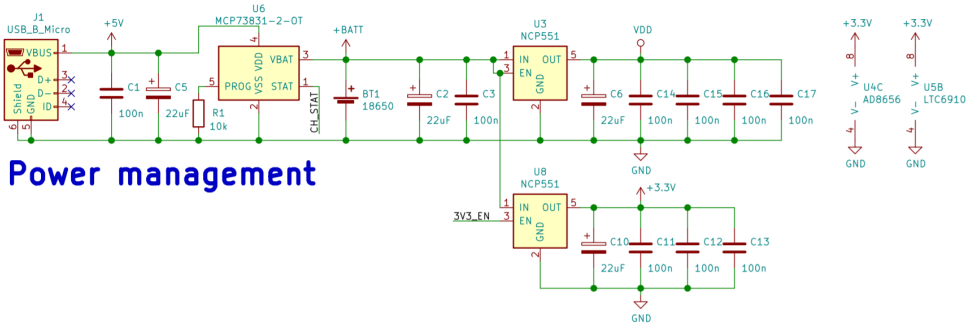

Figure 4.10: Schematic of power management

4.3.1 Battery

There are a lot of available types of batteries nowadays. The device works with 3.3V, so the good choice is to get a battery with operational voltage above this value. The chosen battery is li-ion with a nominal voltage of 3.6V in 18650 type package made by Panasonic. The specifications of the battery are below:[17]

- Type: Lithium-ion rechargeable battery
- Nominal Voltage: 3.6V
- Nominal capacity: Typ. 3350 mAh
- Length: 65.3 mm
- Diameter: 18.5 mm

Charging

Li-ion battery needs a specific charging process. In this case, the process is done by MCP73831 circuit. The charging process is shown in Fig. 4.11 (adapted from [13]). The circuit is powered by 5V from the micro USB connector attached on the PCB. Features of the MCP73831 are listed below:[13]

- Linear Charge Management Controller
- Programmable Charge Current: $15mA$ to $500mA$
- Charge Status Output
- Automatic Power-Down
- Thermal Regulation
- Package: 5-Lead, SOT-23

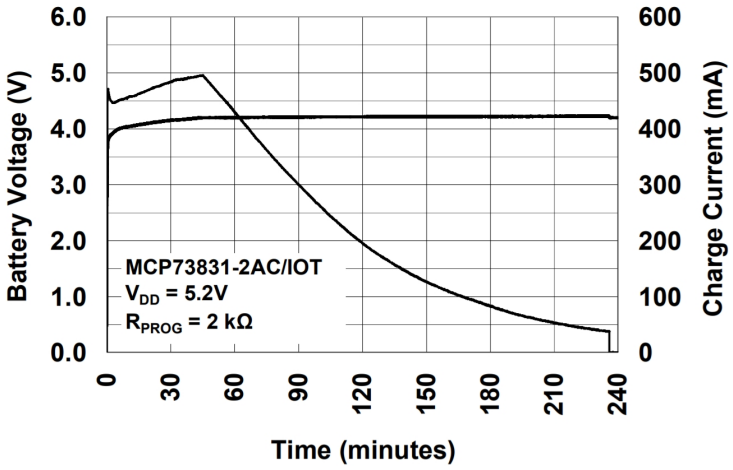

Figure 4.11: Complete Charge Cycle (1000 mAh Li-Ion Battery)

4.3.2 Regulators

As was said before, the whole device works on 3.3V. This voltage is generated by low-drop linear regulator NCP551. The basic features are listed:[15]

- Output voltage: $3.3V$
- Output current: $150mA$
- Low quiescent current of $4.0\mu A$ typical
- High accuracy output voltage of 2.0%
- Built-in enable pin
- Package: 5-Lead, SOT-23

While the device is low-power, the voltage regulator with the low quiescent current was required. There are two LDO to reduce power consumption when the power is in the power-off state. One LDO is powering the MCU itself and the second is powering the rest of the device. The LDO has an enable pin, which controls the output voltage. While the device is in power-off mode, the MCU disables the second LDO. That means that everything except the MCU is not powering. When the MCU is waked up from the low-power mode, the MCU enables the LDO for the rest components.

4.4 LCD

Visualising data of eddy current NDT is usually done by drawing the path of point in an impedance plane diagram diagram (in IQ plane). The position of the point is determined by the imaginary and real part of the RX signal relative to the excitation signal of the TX coil. The second purpose of the display is to set up the device. On display is generated a simple GUI which provides basic settings of the measuring parameters, display parameters and BLE parameters. There is an alternative of the integrated display in the form of Raspberry Pi and its python script.

The driver of the LCD is ST7789VW. The ST7789VW is a single-chip controller/driver for 262K-color, graphic type TFT-LCD. This chip is capable of connecting directly to an external microprocessor. Display data can be stored in the on-chip display data RAM of 240x320x18 bits.[20] List of the basic features of the driver is below:[20]

- Display resolution: 240*RGB (H) *320(V)
- Frame memory size: 240 x 320 x 18-bit = 1,382,400 bit
- LCD driver output circuits
- Interfaces: Parallel 8080-series MCU Interface (8-bit, 9-bit, 16-bit, 18-bit), 6/16/18 RGB Interface, SPI Interface, VSYNC Interface
- Full color: 262K, RGB=(666) max.
- On-chip power system

Displaying unit of the device is a 1.3 inches graphic colour LCD with a resolution of 240x240 pixels. It has 12 pins which provide communication via SPI. It has an integrated LED backlight. The LCD is attached by double-sided tape, its flex connector goes through the PCB and is soldered on the other side of the PCB.

4.5 Bluetooth module

Wireless communication of the measuring device with a master device is mediated by Bluetooth Low Energy (BLE) standard. It uses radio frequency

band internationally reserved for industrial, scientific and medical (ISM) use (2.4 GHz radio frequency band). It is the same band as a classic Bluetooth standard. Similar to classic Bluetooth (BT), BLE uses adaptive frequency hopping spread spectrum to access the shared channel. However, the number of hops is 43 and the channel width is 2MHz as opposed to 79 hops and 1MHz channel width in classic BT. BLE uses a star topology network. Devices using BLE are divided into slave and master. Slave devices are sending advertising packets on dedicated channels, and master devices are looking for them. Once the connection is established, both devices wake synchronously to exchange frames. Both devices are in low power mode rest of the time.[19] The communication is based on sending data via services and characteristics. The topology profile of device's communication is described in the generic access profile (GAP). Data structure are defined in the generic attribute profile (GATT). GATT contains services, and services contain characteristics. Both of these expressions has its own universally unique identifiers (UUID), and they have defined attributes.[16]

Used BLE module is RN4871, and it is made by Microchip. The RN4870/71 BLE module integrates Bluetooth 5.0 baseband controller, on-board Bluetooth stack, digital and analog I/O, and RF power amplifier into one solution.[14] The module's integrated controller is based on 8051 MCU core. Except for these features, the module provides peripheral modules such as SPI interface, ADC converter and much other. The full block diagram of the module is shown in Fig. 4.12 (adapted from [14]).

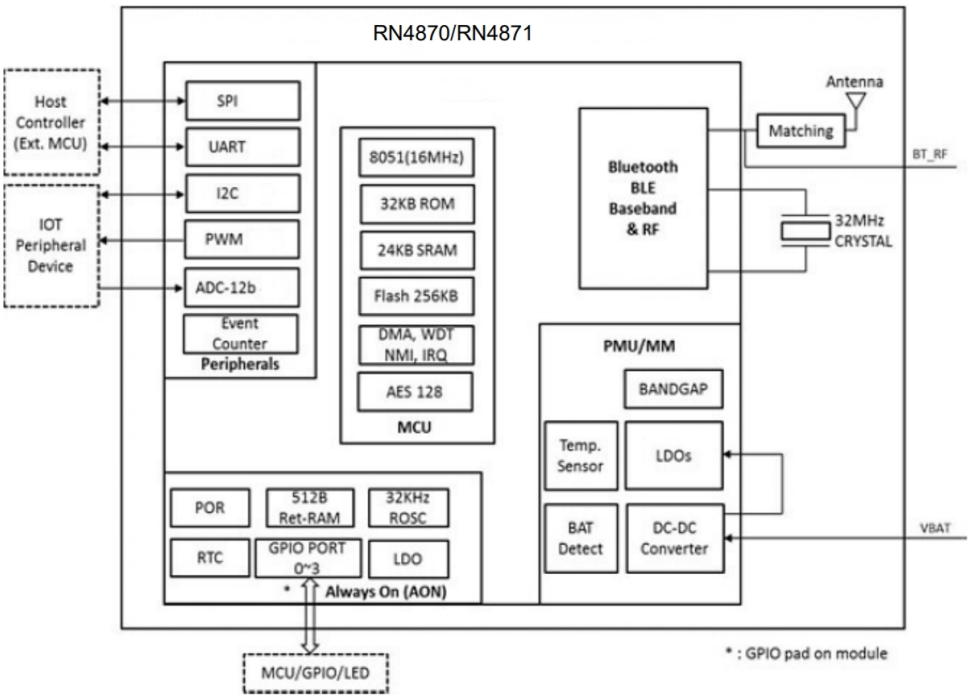

Figure 4.12: Block diagram of the RN4871

The STM32L MCU is communicating with the module via the UART interface. The RN4871 module generates an ASCII command interface, and configuration commands are specified in the module's datasheet. In default mode, the module is using transparent UART service. This service is used in the measuring system. The measuring device is defined as a slave. This module is also used in a supervised device. It is used the same way as in the handheld device, but it is defined as a master. So the desktop device is connecting to the handheld device.

4.6 Overall design

These components are interconnected to create a functional unit. The designed electronics schematic is shown in Fig. 4.13. On the schematic is based the design of the PCB.

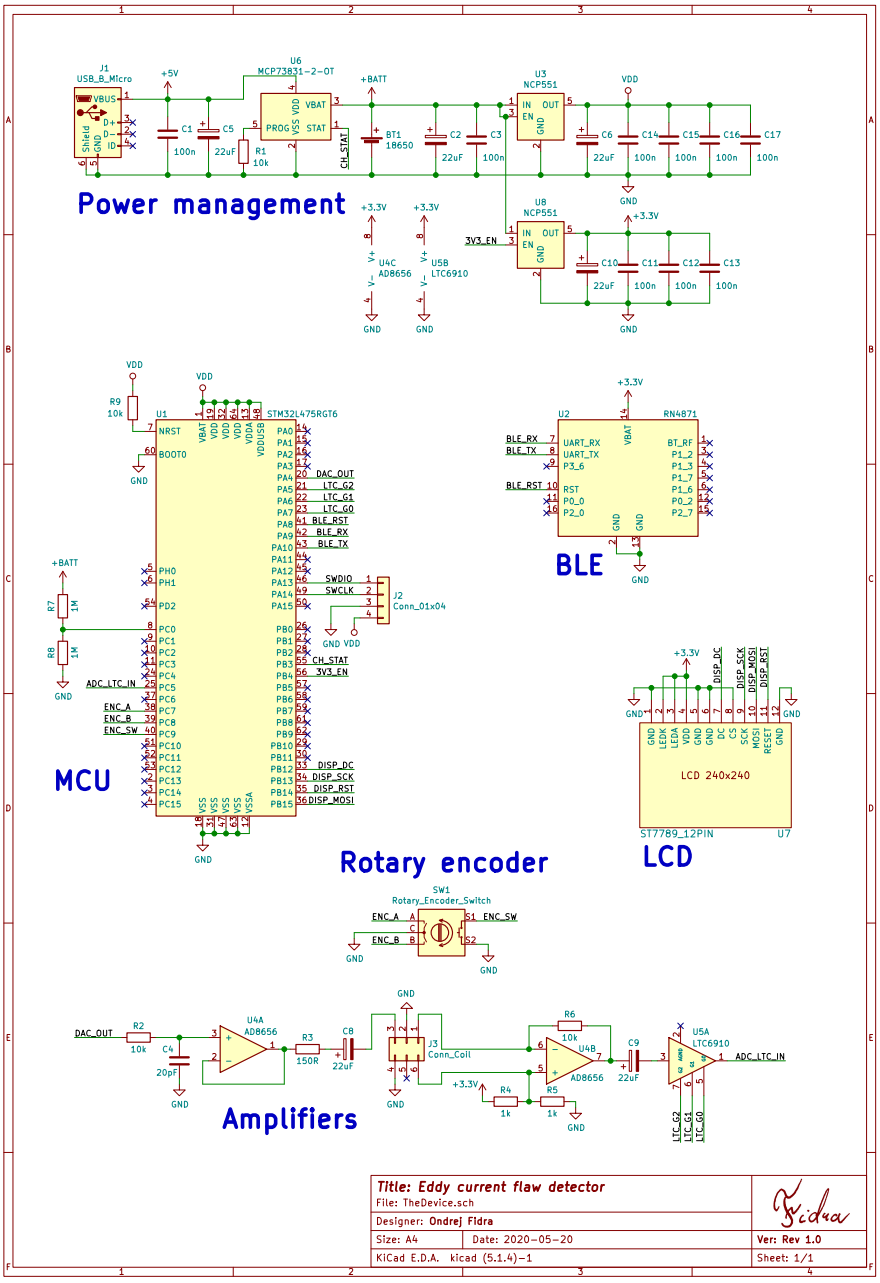

Figure 4.13: Schematic of the device

4.7 Printed circuit board

The main part of the physical construction of the device is based on a double-sided PCB. The PCB is made of a flat substrate from an insulating

material on which are laminated copper foils. The insulating board provides mechanical stability of a device, and the foils provide electrical connection between electronics components. The copper foils are etched by various technologies, such as chemical or mechanical, to make traces and designed shapes on which are the components soldered.

Designing of the PCB was made in a free Electronic design automation (EDA) software KiCAD. It is based on designing PCB according to the schematic design. The schematic must be done before the PCB design starts. The complete schematic can be found in the Appendix section in Fig. 4.13 The dimensions of the PCB are determined by dimensions of the biggest parts of the device. The length is derived from the dimensions of the 18650 battery which has 65 millimetres on length. The battery is placed in the holder, which is approximately 77 millimetres long. The width of the PCB is derived by the LCD, which is 26.2 millimetres wide. The final dimensions are 80 x 26.2 millimetres without rotary encoder and connector for probes. On the shorter sides are soldered rotary encoder and connector for the probe, so the working device is longer. The final design of the PCB of the device is in Fig. 4.14 and Fig. 4.15.

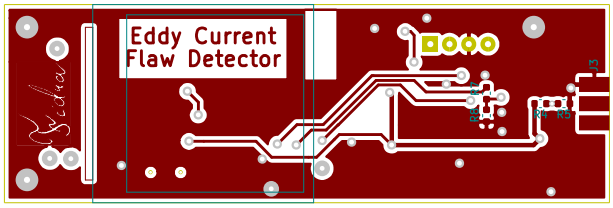

Figure 4.14: Front layer of PCB of the device

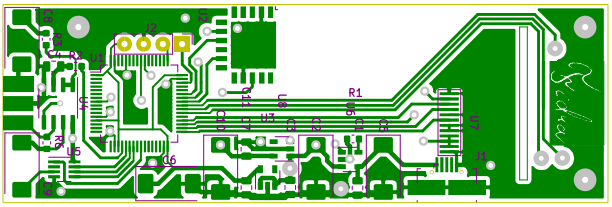

Figure 4.15: Bottom layer of PCB of the device

The photographic method was used to make the PCB. This method begins with applying photoresistive paint to one of the copper layers of the PCB. After the paint is dried, the design is printed on the transparent foil and corrected any visible misprints. The positive picture is then placed on the photosensitive side of the PCB and using the ultraviolet (UV) light the paint is irradiated for about 20 minutes. Meanwhile, the solution of sodium hydroxide ($NaOH$) and water are mixed in a concentration of 7%. The PCB is placed in this solution where the irradiated paint vanishes a uncovers the copper layer. To get off the residue $NaOH$ solution, the PCB is washed under the water. Now, the PCB is ready to etch the copper layer. The iron(III) chloride

($FeCl_3$) is used as an etchant. It takes about another 30 minutes, and the PCB is ready for water wash and for drilling the holes. The same process makes the second side. An acetone dissolvent removes the unwashed paint and as the protective and soldering layer is used rosin dissolved in acetone. When the rosin dries, the PCB is ready for soldering the components.

4.8 Probes

Multiple iterations of probes were made within the thesis. Every iteration has a different design of an arrangement of coils. The aim of making probes for the eddy current testing (ECT) device was to find the best solution in term of sensitivity on tiny cracks in metal. Every probe shares the same general construction that the receiving (RX) coils are wounded on ferrite cores and placed next to each other in anti-serial connection. The TX coil is surrounding the RX coils. The final results are derived from experimental measurements. By the mechanical look, the coils hold together by plastic construction which was designed and produced on a 3D printer.

4.8.1 Version 1

The first probe that was made is with two cylindrical ferrite cores with dimensions of 15 millimetres on the length and 1 millimetre in diameter. The RX coils are wounded on 3D printed frames which have a hole into which is inserted ferrite core. These coils have 300 turns each made by 0.15-millimetre in diameter copper wire. TX coil is also wounded on a plastic frame. Its parameters are: 100 turns with 0.3-millimetre copper wire. The RX coils are inserted into the plastic frame of the TX coil. Between the RX coils and TX coil is aluminium shielding. This set of coils is mechanically fixed by shrink tube. This solution avoids replacing any component of the probe or repair the position of the coils. This coil has a significant error in induced voltage between the two RX coils. Due to this, the resulting signal can not be much amplified and has inadequate sensitivity on small cracks. The made probe is in Fig. 4.16.

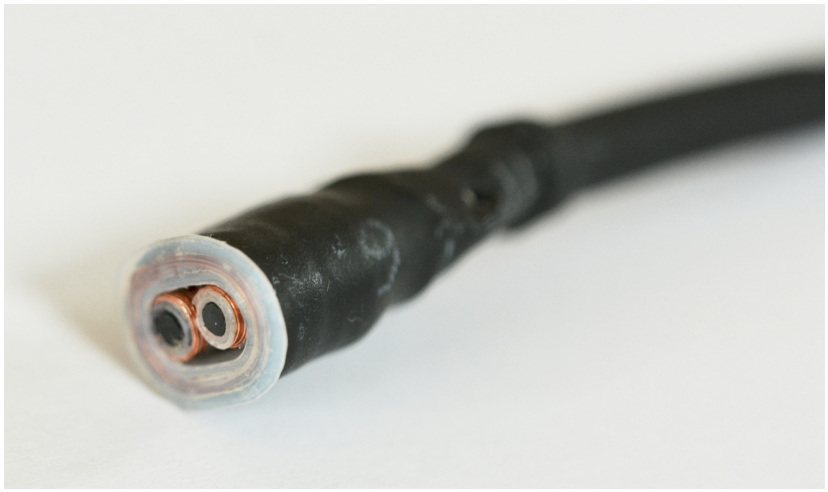

Figure 4.16: Probe version 1

4.8.2 Version 2

The limitations of the first version were improved with the second version. Because of lousy manipulation with small parts from the 3D printer, the first modification was on the dimensions of the probe. In the second version was used ferrite cores with dimensions of 15 millimetres on the length and 4 millimetres in the diameter. Construction is the same as in the first version. RX coils are wounded with 0.2-millimetre copper wire with 200 turns, and the TX coil is wounded with 0.4-millimetre copper wire with 80 turns, they are in Fig. 4.17a. Shielding was made from a transformer sheet metal, and it can be seen in Fig. 4.17b. This modification led to better results. Parameters of RX coils were nearly the same. The only lack was in the way of the more significant dimensions. The probe can be seen in Fig. 4.18.

(a) : Wounded RX coils

(b) : RX coils with shielding

Figure 4.17: Making of the probe version 2

Figure 4.18: Probe version 2

4.8.3 Version 3

The last version of the probes combines both advantages of the previous versions. It uses the same ferrite cores as version one. Compared to this version, the RX coils are directly wounded on these cores. After the winding, the coils were measured by L-meter and eventually adjusted to the same value of inductance. Fixing RX coils was made by cyanoacrylate based glue. The only 3D printed part is a frame for the TX coil. The multiple TX coils were made and compared to get the best sensitivity. The manufacturing of coil is never ideal, and parameters differ. The aim of the making of multiple versions of coils is in to find the best compromise. The making process of these coils is shown in Figs. 4.19a, 4.19b, 4.20a, 4.20b. The final assembled coil with connector is in Fig. 4.21.

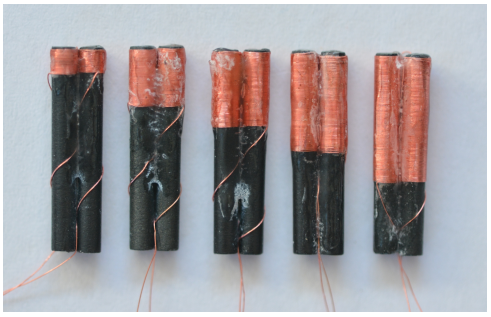

(a) : Various RX coil of version 3

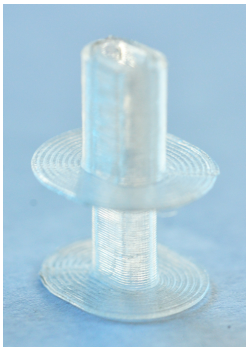

(b) : 3D printed frame of TX coil

Figure 4.19: Making of the probes version 3

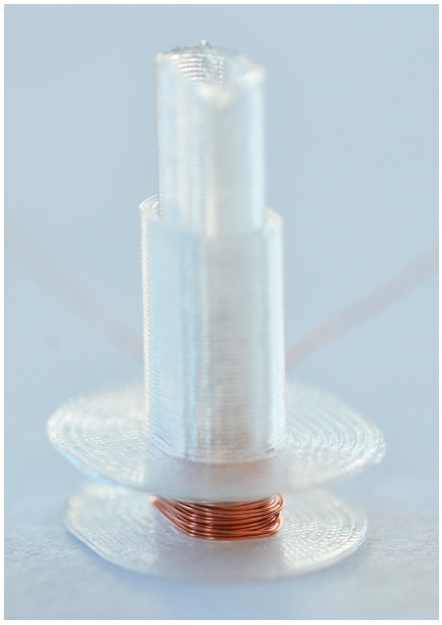

(a) : Wounded TX coil on a 3D printed frame

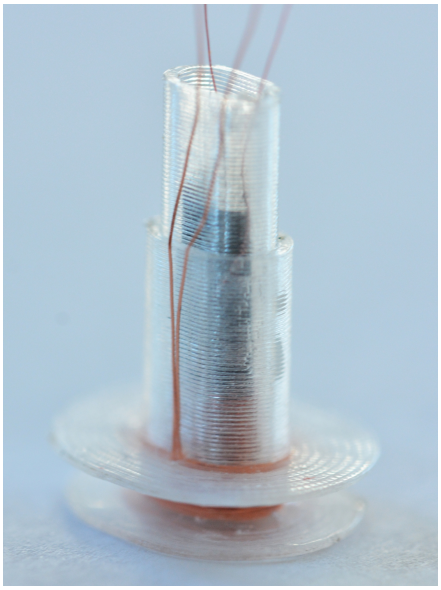

(b) : Probe with RX coils in TX frame

Figure 4.20: Making of the probes version 3

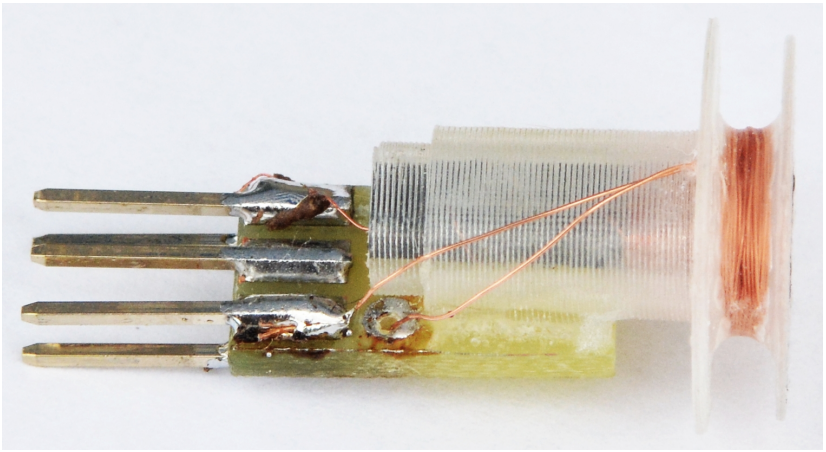

Figure 4.21: Probe version 3 attached on the connector

4.9 Plastic parts

Another component in the mechanical stage of the thesis is plastic parts. These parts were designed in Computer-aided design (CAD) software named FreeCAD. When the parametric objects were designed, the stereolithography (STL) files were generated which stands as an input format for the 3D printer slicer software Simplify3D. This software generates instructions in 4-dimensional space (three dimensions for moving and one dimension for the

amount of material) for the 3D printer in G-code language.

FreeCAD is a multi-platform, free and open-source, parametric 3D CAD modeller. It provides a wide range of purposes of usage. In the thesis, FreeCAD was used to model solids for the mechanical part of the device, concretely to design the 18650 battery holder, the covering of the device and frames for the coils. When the pieces are designed, the FreeCAD provides a plugin to generate STL files (Mesh Designer). The design of the battery holder is shown in Fig. 4.22.

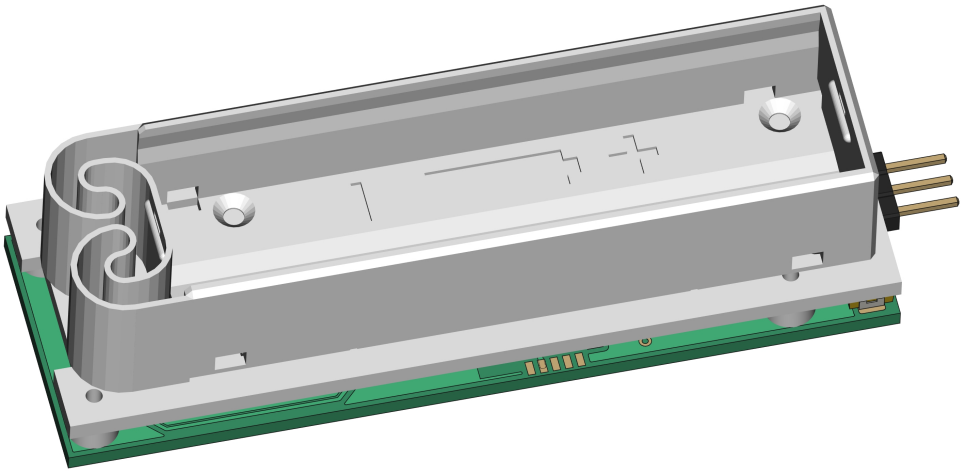

Figure 4.22: Design of battery holder

Next step belongs to slicer software Simplify3D. The exported STL files from the FreeCAD can be loaded in Simplify3D and, by the printer-specific setting, it generates instructions for the 3D printer. They are written in G-code language and consists of linear paths with accelerations and speeds in 3-dimensional space and extruder information about the amount of supplied material along this path. Sliced design of coil's frame is in Fig. 4.23 (this case uses vase mode). The final print of the battery holder is in Fig.

To make from the designed and exported data a physical parts the 3D printer was used. It is made from the mainframe with a movable axis which provides 3 degrees of freedom. The plastic material is derived in the form of a string, also filament, which is wounded on a spool. It goes through an extruder, a system, which melts the filament and through a nozzle is material derived into the place. The extruder has its stepper motor to control the flow of the material. The 3D printed battery holder is in Fig. 4.24.

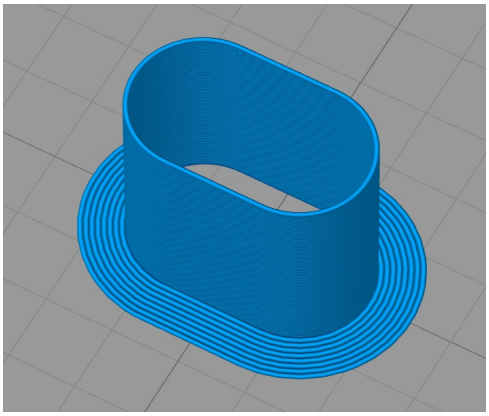

Figure 4.23: Coil frame prepared to print by slicing

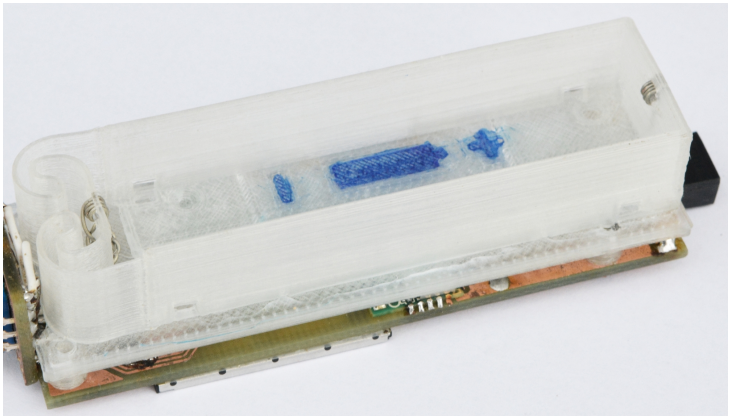

Figure 4.24: 3D printed battery holder

4.10 Raspberry Pi

As a superior system for the measuring system is used. It is a single-board computer running on Raspbian, the free operating system based on Debian. The Raspberry Pi3 B+ is used in the thesis. Its main features are the following:[9]

- Broadcom BCM2837B0, Cortex-A53 (ARMv8) 64-bit SoC @ 1.4GHz
- 1GB LPDDR2 SDRAM
- 2.4GHz and 5GHz IEEE 802.11.b/g/n/ac wireless LAN, Bluetooth 4.2, BLE
- Extended 40-pin GPIO header
- 4 USB 2.0 ports

- DSI display port for connecting a Raspberry Pi touchscreen display
- Micro SD port for loading your operating system and storing data

It is used an LCD display with touchscreen for the Raspberry Pi used in the thesis. The display has 800 x 480 pixels resolution, and it has 7 inches in diagonal. The LCD has a mechanism to attach the Raspberry, so the single unit computer was created. The Raspberry Pi provides a BLE interface, but there was a problem with the compatibility of the BLE module. Because of this, the reduction for RN4871 was made to connect to the Raspberry's pin header. Raspberry Pi has RN4871 module connected on pins GPIO14 (TX), GPIO15 (RX) and GPIO2 (RST). For the mechanical stability, a PCB was made to Raspberry's pin header. The design of the PCB is shown in Fig. 4.25. The whole setup is shown in Fig. 4.26.

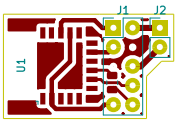

Figure 4.25: Raspbery Pi external BLE module

Figure 4.26: Raspbery Pi with LCD and BLE module

Chapter 5

Software

Intangible section of the thesis is its software. In this chapter, the software (SW) written for the thesis is described. It can be divided into two elementary parts, SW for the handheld device (MCU) and SW for the desktop device (Raspberry Pi).

5.1 MCU

Integrated development environment (IDE) named Eclipse was used to write the program for the MCU. This IDE has installed expanding platform for developing apps for the STM32 type microcontrollers named STM32CubeIDE. Project for the STM32L475 is written in C programming language. There were not used external libraries for controlling peripherals by the third party. All of the libraries were written primarily for the thesis.

The task of the MCU's software is to control, compute and represent captured data. It begins on generating waveforms for the TX coil and simultaneously to this job save the converted signal from the RX coils. Then, the implementation of the lock-in amplifier is computing this data to get imaginary and real components of the signal. The last step of this measuring chain is to represent or send data. Representing data is done on display in the form of drawing the path of the computed data from lock-in. Except for this task, the MCU is generating and serving graphical user interface (GUI), which provides settings of the measurements parameter and device setting

such as displaying parameters and BLE settings.

5.1.1 Sampling

The flow of the code determined to control the data sampling is represented in Fig. 5.1. In this text, the description is provided for this flowchart. First operations what the code does is concerned with DAC and ADC peripheral initialisation. This process is related to the setup of the basic timer TIM6 and DMA peripheral. DAC peripheral is configured to be triggered on the TIM6 event and to be fetched via DMA peripheral. The similar process is done on ADC. To acquire simultaneously sampled data, the source of the trigger is the same as the DAC (timer TIM6). Saving data from this peripheral to memory is done using DMA. The DMA peripheral is transferring data for DAC and ADC. In the case of DAC, the dedicated DMA channel sends data to the peripheral from allocated memory. To accomplish continuous data fetching and generating continuous waveforms, the DMA is configured in circular mode. For the ADC peripheral is a dedicated channel configured for transferring data from peripheral to memory. The single conversion has a length of one period of the waveform, so the DMA is configured as a non-circular. Configuration of TIM6 is done by enabling trigger output (TRGO). The prescaler (PSC) and auto-reload register (ARR) defines the sampling rate of the DAC. Values of both registers differ by the set frequency. After these peripheral are ready, the computation of waveform samples and saved in specified memory space is done. In this case, the device can generate sinusoidal waveforms. The number of points and values depends on the frequency and amplitude parameters. In this point, the DAC can be turned on, and the sampling can start. Once the request to start sampling is given, the interrupt from the DMA channel, dedicated for DAC, on the transfer done event is enabled, to get the beginning of the period. In this interrupt is enabled sampling of the ADC peripheral, and the interrupt from DMA ADC channel is enabled. Once all of the ADC conversions are done, the sampled data are added to a global variable designed for future averaging. This process repeats until all periods are sampled. At this point, the sampling is done, and average values can be computed. Now, the data are valid.

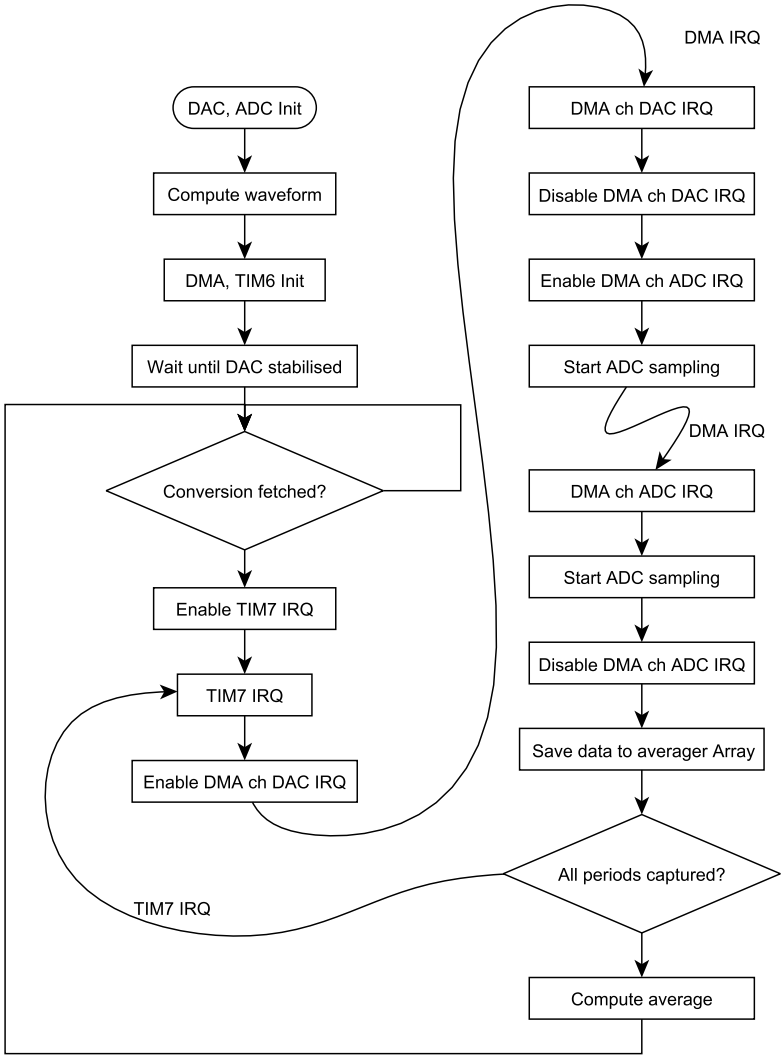

Figure 5.1: Sampling program flow

5.1.2 Data processing

A digital lock-in amplifier is implemented to get representable data from sampled ones. Flowchart of implementation is in Fig. The first operation, as can be seen in the flowchart, is to compute the mean value from the samples data. The program flow then goes to the cycle, where the computed mean value subtracts all the samples. These values are then multiplied with corresponding points of sinusoidal and cosinusoidal functions. The results are saved in two arrays. From these arrays are computed mean values, after the cycle. This procedure implements a low-pass filter. These two mean values correspond to a real and an imaginary component of the signal. The values are saved into the arrays and can be represented.

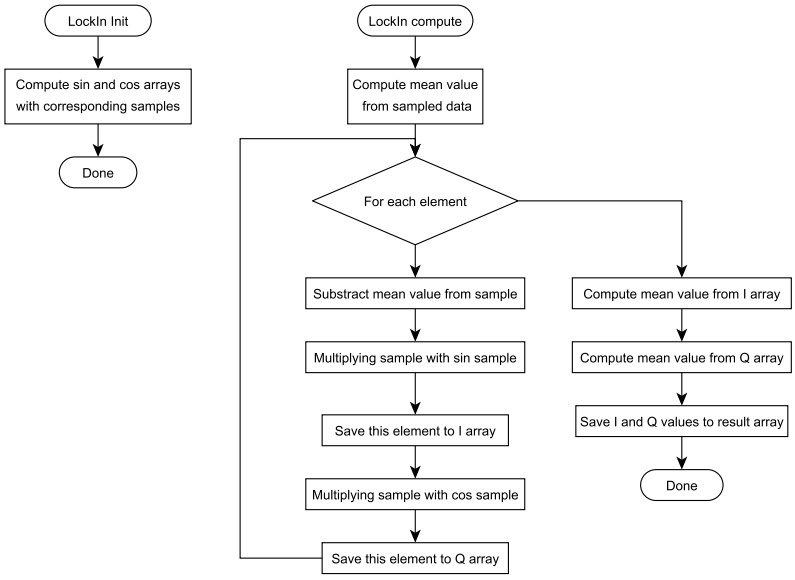

Figure 5.2: Data processing program flow

5.1.3 User interface

The mission of the user interface is to generate and serve a human-machine interface (HMI). It represents measured data and enables to change parameters of the device. The interacting element of HMI is a rotary encoder, which is placed on the handheld device. The user interfaces define four types of events from the rotary encoder. They are rotate left, rotate right, short press and long press. The input pins are configured on interrupts via EXTI peripheral, to catch these events. The interrupts are generated when a change on pins come. Logic statements in interrupts then decide what type of event it is. There is an attached timer (TIM4) with three capture compare channels enabled, to prevent generating false-positive events. The interrupts of these channels are preventing to take unwanted bouncing of the contact of the rotary encoder. The corresponding events are stored in the status register. The main thread of the program is cyclically checking the state of this status register. When an event comes, the program reaction is based on the actual page and marked line. On the end of this event is called the UI updating service. A particular element of the UI is a continuous measuring and representing data on display.

5.2 Raspberry Pi

As a desktop device for data representing is used Raspberry Pi. The software which draws the path of the measured data is written in Python 3.7 language. To get work with the Bluetooth module (RN4871) is used internal UART communication. Its pins are on embedded pin header. For communication with the module, the library named pyserial is used. Received data from the Bluetooth module must be modified and stored in lists. For the modification of data, the library named numpy is used. And finally, for the plotting graph, the library named matplotlib is used. Program flow of the data getting and data representation is shown in Fig. 5.3.

First of all, the program initialises serial communication for the module. Then the module resets via its hardware reset pin. Optionally, the factory resets can be done. The module is then configured with the required parameters. The configuration includes software resets to update variables. After that, the module tries to connect to the handheld device. The output of the module is testing for the string "%STREAM_OPEN%", which means that the Raspberry Pi can communicate with the handheld device. Now, the plot is being ready to draw the data from lists. The handheld device immediately sends measured data in raw 4-byte float format. The code reads it and saves it into the list. The plot is then updated with new data.

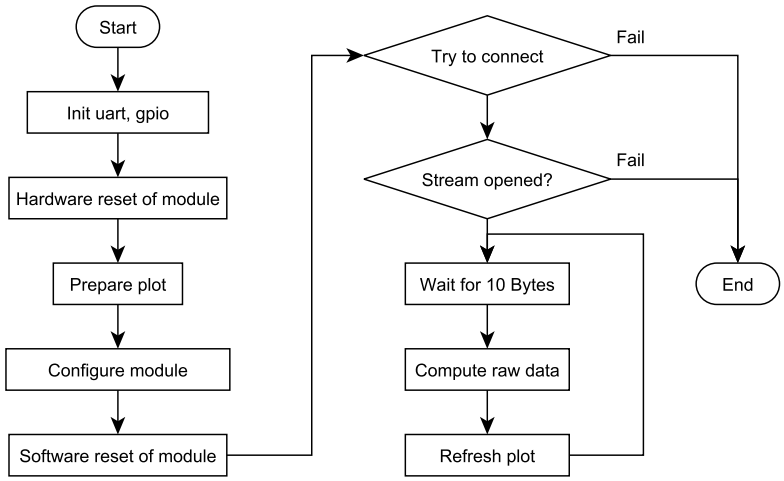

Figure 5.3: Flowchart of Raspberry Pi program

Chapter 6

Results

Within this thesis was created a measuring system for eddy current testing techniques. The solution consists of the battery-powered handheld device with replacement probes, several types of probes and desktop visualisation system. This chapter describes these parts from their functionality and how they were made. The aluminium sheet with artificial flaws was made for the evaluation of detectability of the device.

6.1 The device

On the beginning of the evaluation was created a prototype device to test a various design of components. The prototype was built on universal PCB. The developing of the device took place step by step. First The DAC with excitation amplifiers were designed, then the ADC part was designed. When the data were sampled, the development of LIA and GUI was made. The final design of the device is based on the gained knowledge from the prototype device. The prototype device with all of the components is shown in the Appendix section in Fig. A.1.

When the prototype's design was debugged, the designing of the final version started. Schematic design of the final device can be found in the Appendix section in Fig. 4.13. From the schematic, the PCB was designed and made. The photos of the manufacturing of the device can be found in the Appendix section in Figs. A.2, A.3, A.3, A.5, A.6. Then the PCB was

mounted with components and MCU programmed. At final, the device got a battery holder, and the case was attached. The complete handheld device is shown in Fig. 6.1.

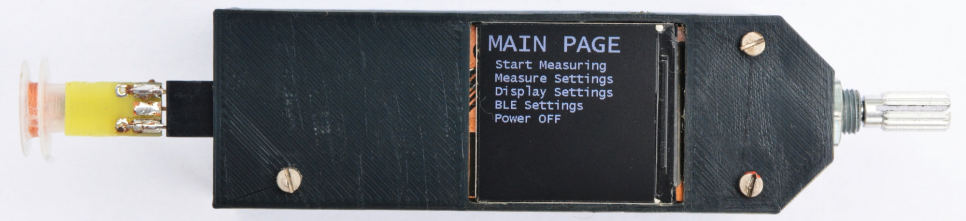

Figure 6.1: Final handheld device

The device's functionality provides to an operator set the parameters critical for ECT. The setting is made by GUI on its display. Among the settable parameters belong frequency and amplitude of excitation signal, the number of averaging periods, gain of receiving op-amp. These parameters setup the measurement variables. Parameters, which are settable and serves for display settings are enabling/disabling drawing received waveform, IQ plane, the scale of IQ plane, shading feature enable/disable and the number of points of shading feature. The last settable parameter belongs to turn on/off BLE peripheral. Several screens of the GUI do the setting, and parameters changing is done by rotary encoder. All of the available screens of the device are shown in Fig. 6.2.

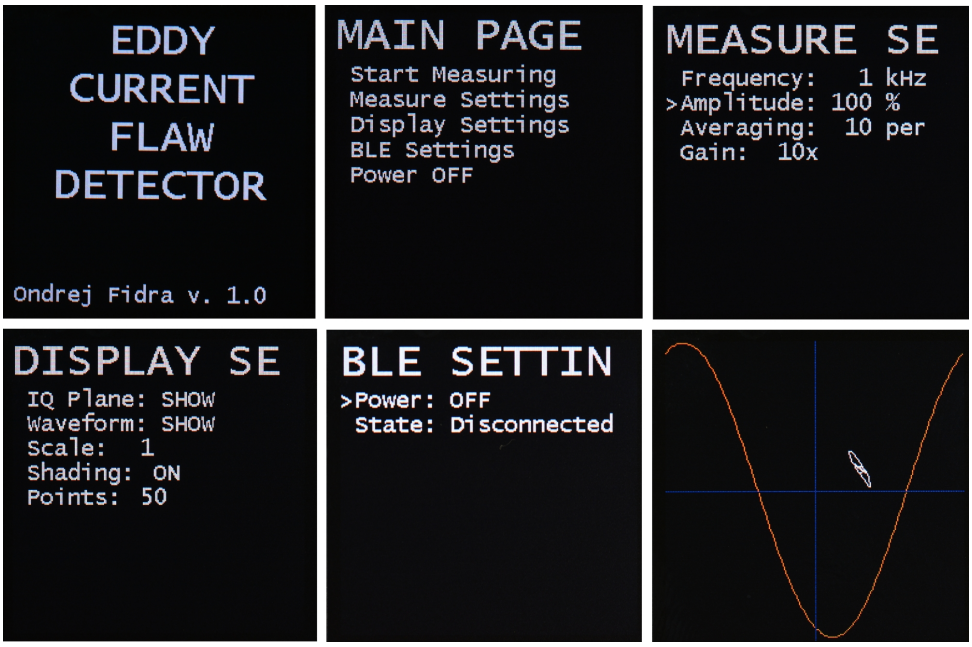

Figure 6.2: Screens of the device's GUI

The handheld device cooperates with a desktop station based on Raspberry Pi. It provides data representation on a 7 inches LCD. The example of data representation on Raspberry Pi is shown in Fig. 6.3, where is detected

artificial flaw type hole. Eventually, there is a possibility to export measured data via a Python script. The whole composition is in Fig. 6.4.

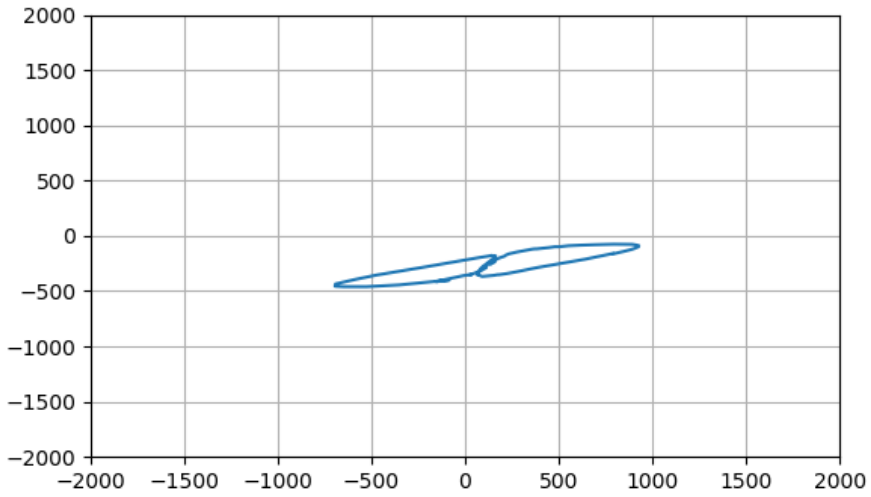

Figure 6.3: The detail of a graph generated on Raspberry Pi

Figure 6.4: The ECT measurement system

6.2 Probes

An inseparable part of the ECT measurement device is a probe. Within this thesis was created 3 versions of differential probes. Its construction is

described above in section 4.8. The resulting sensitivities of the coils were determined by detecting artificial flaws. The testing subject can be seen in Fig. 6.5. It is a sheet of duralumin sheet with drilled holes as artificial flaws. It consists of one hole of diameter 4 millimetres, two smaller holes with diameter 2 millimetres and 3 holes with diameters of 1, 0.8, 0.6 millimetres. The coil version 1 has poor balanced RX coils, so the high gain can not be used. Thus it is not able to detect smaller holes than 2 millimetres. Probe version 2 is well balanced, but its disadvantage is in its dimensions. The high gain could be used. Nevertheless, it could not be able to detect smaller holes than 2 millimetres. Version 3 probes combined small dimensions and well balanced RX coils. It could visualise all of the available types of flaws created on the sheet. The response of the measuring device on different types of holes can be seen in Fig. 6.6.

Figure 6.5: Testing sheet of metal with artificial flaws

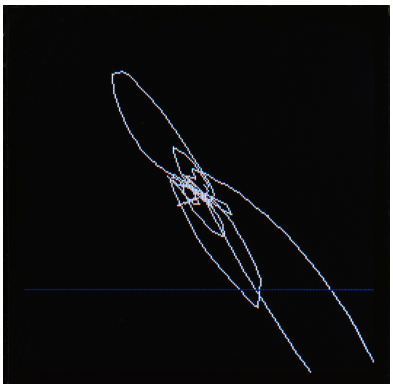

Figure 6.6: Result of the measurement of more flaws

Chapter 7

Conclusion

This thesis provides a description of designing and making the measurement system for eddy current testing. The wireless, battery-powered handheld device was designed and manufactured, and stationary visualisation unit communicating wirelessly with the handheld device was made. The handheld device features a probe changing mechanism, to use various types of probes for various types of detectable flaws. The several types of probes with different parameters were made.

The handheld device is based on STM32L475RG microcontroller. It does the requiring signal generating, the computation of software lock-in amplifier and signal processing. The device is designed to generate excitation signal and to sample received signal from the probe. For this purpose, the circuits with operational amplifiers are in the device. It contains the LCD display to represent the results of the measurement. Thus, the device can be used with or without the visualisation unit. For wireless data transferring with visualisation stationary unit, the Bluetooth low energy communication is used. The device has a rotary encoder for setting purposes.

Within the thesis, several types of probes were made. For the testing of the device and probes, the metal sheet with artificial flaws was made. It is made from duralumin sheet with drilled holes. The response of the device on the flaws is the same as known responses from the literature. The probes are differential type consisting of receiver coils that are based on ferrite cores and excitation coil that is wounded around the RX coils.

The visualisation unit is based on a Raspberry Pi computer with LCD

display module. It runs a Python script to communicate with the device and to visualise measured data in a plot.

7.1 Future work

In the future, the device will offer a user-defined excitation waveform. There will be a possibility to choose where the data would be computed. And the possibility of raw data exporting will be implemented to perform various algorithms based on artificial intelligence or likelihood computation.

Appendix A

The device

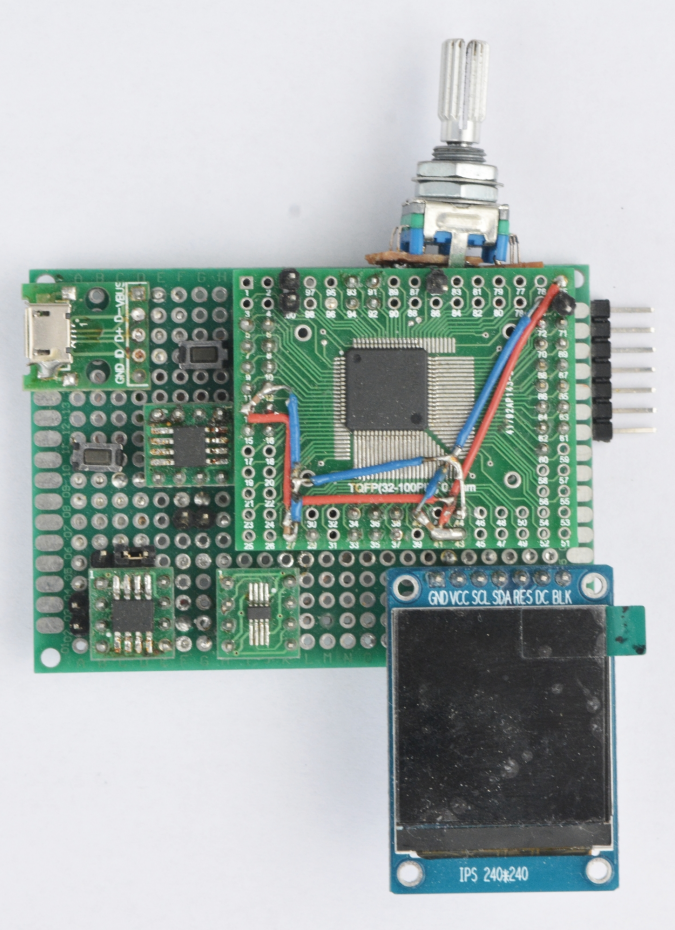

Figure A.1: Front side of the prototype

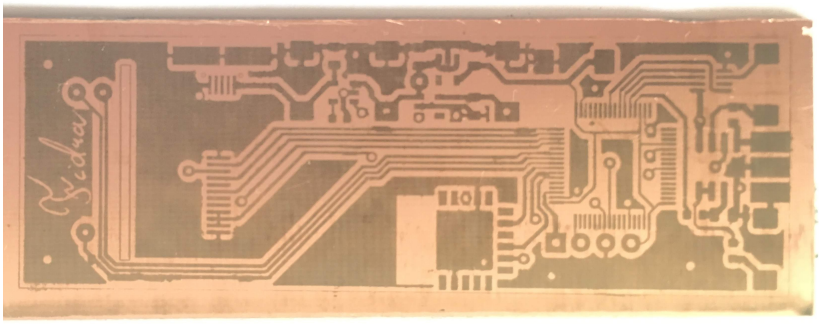

Figure A.2: PCB ready to be etched

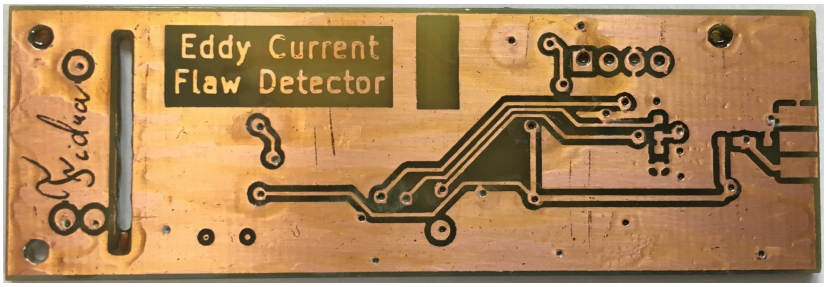

Figure A.3: Front side of the etched PCB

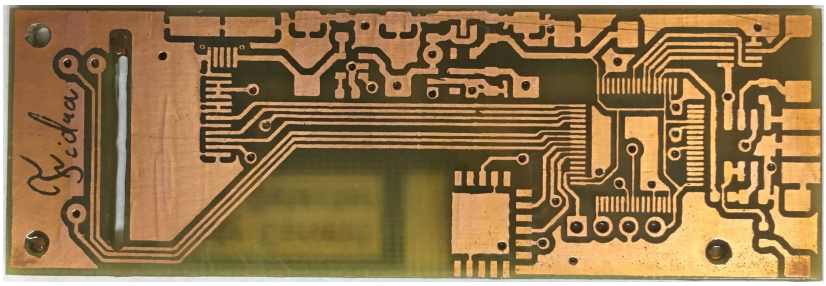

Figure A.4: Back side of the etched PCB

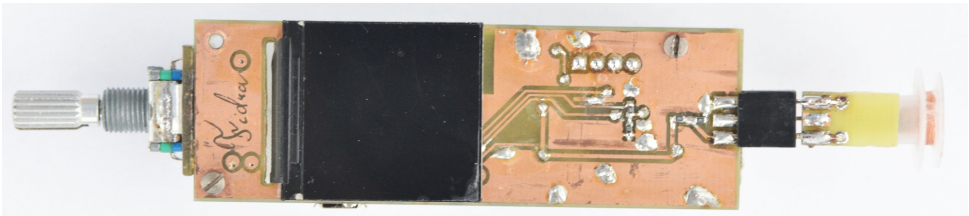

Figure A.5: Front side of the soldered PCB

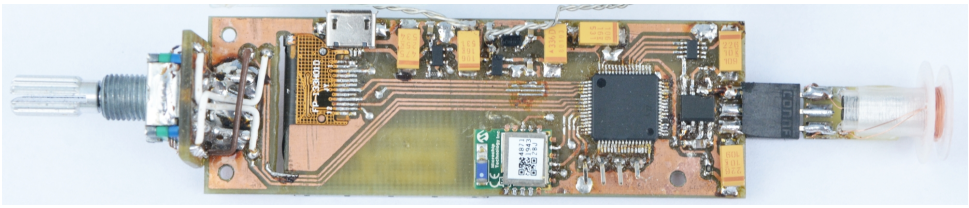

Figure A.6: Back side of the soldered PCB

Appendix B

Bibliography

[1] J. Aguirre, N. Medrano, B. Calvo, S. Celma, and C. Azcona. An analog lock-in amplifier for embedded sensor electronic interfaces. *20th European Conference on Circuit Theory and Design (ECCTD)*, 2011.

[2] Analog devices. *AD8655/AD8656, Low Noise, Precision CMOS Amplifier, D05304-0-10/13(E)*, October 2013. Rev E.

[3] Analog devices. *LTC6910-X, Digitally Controlled Programmable Gain Amplifiers in SOT-23, 6910123fb*, June 2017. Rev B.

[4] S. Bhattacharyya, R. N. Ahmed, B. B. Purkayastha, and K. Bhattacharyya. Implementation of digital lock-in amplifier. *Journal of Physics: Conference Series 759 (2016) 012096*, 2016.

[5] NDT Education Resource Center. About ndt. `https://www.nde-ed.org/AboutNDT/aboutndt.php`. Accessed: 2020-05-21.

[6] NDT Education Resource Center. Depth of penetration and current density. `https://www.nde-ed.org/EducationResources/CommunityCollege/EddyCurrents/Physics/depthcurrentdensity.htm`. Accessed: 2020-05-18.

[7] NDT Education Resource Center. Mutual inductance. `https://www.nde-ed.org/EducationResources/CommunityCollege/EddyCurrents/Physics/mutualinductance.htm`. Accessed: 2020-05-18.

[8] NDT Education Resource Center. Ndt intro. `https://www.nde-ed.org/EducationResources/CommunityCollege/NDTIntro/cc_intro001.htm`. Accessed: 2020-05-18.

[9] Raspberry Pi Foundantion. Raspberry pi 3 model b+. https://www.raspberrypi.org/products/raspberry-pi-3-model-b-plus/. Accessed: 2020-05-16.

[10] J. García-Martín, E. Vázquez-Sánchez, and J. Gomez-Gil. Non-destructive techniques based on eddy current testing. *Sensors 2011*, 2011.

[11] J. Gaspara, S. F. Chenb, A. Gordillob, M. Heppb, P. Ferreyraa, and C. Marqués. Digital lock in amplifier: study, design and development with a digital signal processor. *Microprocessors and Microsystems 28 (2004)*, 2004.

[12] Zurich Instruments. Principles of lock-in detection. https://www.zhinst.cn/china/tw/resources/principles-lock-detection. Accessed: 2020-05-18.

[13] Microchip. *MCP73831/2, Miniature Single-Cell, Fully Integrated Li-Ion, Li-Polymer Charge Management Controllers, DS20001984G*, July 2014. Rev G.

[14] Microchip. *RN4870/71, Bluetooth® Low Energy Module, DS50002489D*, April 2019. Rev D.

[15] ON Semiconductor®. *NCP551, Voltage Regulator - CMOS, Low Iq, Low-Dropout*, October 2019. Rev 19.

[16] O'Reilly. Chapter 4. gatt (services and characteristics). https://www.oreilly.com/library/view/getting-started-with/9781491900550/ch04.html. Accessed: 2020-05-15.

[17] Panasonic®. *Lithium Ion, NCR18650B*, 2012. V13.11 R1.

[18] Peter J. Shull, editor. *Nondestructive Evaluation Theory, Techniques, and Applications*. Marcel Dekker, Inc., 2002.

[19] M. Siekkinen, M. Hiienkari, J.K. Nurminen, and J. Nieminen. How low energy is bluetooth low energy? *WCNC, Embracing Machine-to-Machine Communications and Beyond*, 2012.

[20] Sitronix Technology Corporation. *ST7789VW*, September 2017. V1.0.

[21] STMicroelectronics. Stm32l475rg. https://www.st.com/content/st_com/en/products/microcontrollers-microprocessors/stm32-32-bit-arm-cortex-mcus/stm32-ultra-low-power-mcus/stm32l4-series/stm32l4x5/stm32l475rg.html. Accessed: 2020-05-14.

[22] STMicroelectronics. *STM32L475xx, DS10969*, March 2019. Rev 5.

[23] STMicroelectronics. *STM32L47xxx, STM32L48xxx, STM32L49xxx and STM32L4Axxx advanced Arm®-based 32-bit MCUs, RM0351*, April 2020. Rev 7.

Appendix C

CD